Multicompartment polyion complex micelles based on triblock polypept(o)ides mediate efficient siRNA delivery to cancer-associated fibroblasts for antistromal therapy of hepatocellular carcinoma

Schneider, P.; Zhang, H.; Simic, L.; Dai, Z.; Schroers, B.; Akilli-Oeztuerk, O.; ... ; Barz, M.

ADVANCED MATERIALS
www.advmat.de

Multicompartment Polyion Complex Micelles Based on Triblock Polypept(o)ides Mediate Efficient siRNA Delivery to Cancer-Associated Fibroblasts for Antistromal Therapy of Hepatocellular Carcinoma

Paul Schneider, Heyang Zhang, Leon Simic, Zhuqing Dai, Barbara Schrörs, Özlem Akilli-Öztürk, Jian Lin, Feyza Durak, Jenny Schunke, Vanessa Bolduan, Bram Bogaert, David Schwiertz, Gabriela Schäfer, Matthias Bros, Stephan Grabbe, Jörn Markus Schattenberg, Koen Raemdonck, Kaloian Koynov, Mustafa Diken, Leonard Kaps,* and Matthias Barz**

Hepatocellular carcinoma (HCC) is the most frequent type of primary liver cancer and the third leading cause for cancer-related death worldwide. The tumor is difficult-to-treat due to its inherent resistance to chemotherapy. Antistromal therapy is a novel therapeutic approach, targeting cancer-associated fibroblasts (CAF) in the tumor microenvironment. CAF-derived microfibrillar-associated protein 5 (MFAP-5) is identified as a novel target for antistromal therapy of HCC with high translational relevance. Biocompatible polypept(o)ide-based polyion complex micelles (PICMs) constructed with a triblock copolymer composed of a cationic poly(L-lysine) complexing anti-MFAP-5 siRNA (siMFAP-5) via electrostatic interaction, a poly(γ-benzyl-L-glutamate) block loading cationic amphiphilic drug desloratatine (DES) via π–π interaction as endosomal escape enhancer and polysarcosine poly(*N*-methylglycine) for introducing stealth properties, are generated for siRNA delivery. Intravenous injection of siMFAP-5/DES PICMs significantly reduces the hepatic tumor burden in a syngeneic implantation model of HCC, with a superior MFAP-5 knockdown effect over siMFAP-5 PICMs or lipid nanoparticles. Transcriptome and histological analysis reveal that MFAP-5 knockdown inhibited CAF-related tumor vascularization, suggesting the anti-angiogenic effect of RNA interference therapy. In conclusion, multicompartment PICMs combining siMFAP-5 and DES in a single polypept(o)ide micelle induce a specific knockdown of MFAP-5 and demonstrate a potent antitumor efficacy (80% reduced tumor burden vs untreated control) in a clinically relevant HCC model.

1. Introduction

Hepatocellular carcinoma (HCC) is the most frequent type of primary liver cancer and is the third leading cause of cancer-related deaths in the world. Only in Europe, HCC accounts for more than 745 000 deaths annually. Liver cirrhosis caused by chronic liver inflammation (e.g., due to chronic viral hepatitis or steatotic liver disease) is the strongest risk factor for this type of cancer and such patients have a yearly risk of ≈6% to develop HCC.[1–3] Conventional chemotherapy is futile and for a long time sorafenib, a tyrosine-kinase inhibitor (TKI), was the only approved drug for HCC patients in an advanced stage. Nowadays, combinatorial biologic therapies (e.g., Atezolizumab (anti-PD-L1) with Bevacizumab (anti-VEGF)) and novel TKI improved the therapeutic situation,[4,5] but survival prognosis remain modest and novel drugs are urgently needed. Novel therapeutic strategies take advantage of a deeper understanding of the mutational landscape of HCC, which has been gained in the recent decade. In this process, the tumor microenvironment (TME) has gained

The ORCID identification number(s) for the author(s) of this article can be found under https://doi.org/10.1002/adma.202404784

DOI: 10.1002/adma.202404784

P. Schneider, L. Simic, J. Schunke, V. Bolduan, D. Schwiertz, G. Schäfer, M. Bros, S. Grabbe, L. Kaps, M. Barz
Department of Dermatology
University Medical Center of the Johannes Gutenberg-University
55128 Mainz, Germany
E-mail: leonard.kaps@uks.eu; m.barz@lacdr.leidenuniv.nl

the attention of oncologists.[6,7] HCC modulates adjacent immune cells, stromal cells, blood vessels, and extracellular matrix to form an immunosuppressive TME.[8] Cancer-associated fibroblasts (CAF) are the predominant cell type in the stromal compartment of the TME. They play critical roles in HCC progression, such as guiding tumor cells for invasion and migration or modulating the extracellular matrix, thereby facilitating new vessels, and suppressing antitumor immunity.[9] Due to the manifold tumor-promoting roles, CAF have emerged as an interesting target for antistromal therapies.[10–12] Microfibrillar-associated protein 5 (MFAP-5) is an interesting CAF-specific target in solid tumors. It is a key component of elastic microfibers in the extracellular matrix, promoting neoangiogenesis due to the regulation of endothelial cell (EC) behaviors.[13–15] This is vital for solid tumors as they rely on new established vascular beds to satisfy their increasing metabolic demand of nutrients and oxygen to facilitate progressive growth and metastasis.[16] In addition, it was reported that CAF-derived MFAP-5 can directly interact with carcinoma cells to drive tumor invasion and migration.[14,17] Therefore, CAF-derived MFAP-5 is a promising target for hypervascularized solid tumors like HCC.[18]

Small interfering RNA (siRNA) has demonstrated an enormous therapeutic potential by suppressing disease-associated protein production via RNA interference (RNAi) for a wide variety of diseases.[19] However, some obstacles including poor pharmacokinetics, rapid excretion of siRNA via the urinary tract, and fast degradation by RNases in the body limit its application.[20] To overcome these limitations, extensive research has been devoted to the development of nano-formulations (e.g., lipid nanoparticles (LNPs), polymers) or conjugates (e.g., *N*-acetylgalactosamine (GalNAc)-conjugates) to achieve efficient gene knockdown.[21–23] Nevertheless, entrapment of nano-formulations in the endosomal compartments after cell uptake remains a hurdle in siRNA delivery. Several strategies have been explored to enhance the endosomal escape via endosomal membrane fusion or disruption.[24,25] Cationic amphiphilic drugs (CADs), such as nortriptyline, lofepramine, and ebastine, have been previously used to boost endosomal escape via transient induction of lysosomal membrane permeabilization.[26–28]

In our previous work, polypept(o)ide-based ABC-triblock copolymers with different combinations of blocks have been demonstrated to form biocompatible polyion complex micelles (PICMs) for siRNA delivery.[29] Polypept(o)ides, polypeptoid-*block*-polypeptide copolymers, are synthetic polymers, which are based on endogenous amino acids and combine the diversity of polypeptides with the stealth properties of the polypeptoid polysarcosine (pSar) in a block copolymer.[30,31] They are synthetically accessible by sequential nucleophilic ring-opening polymerization (ROP) of *N*-carboxyanhydrides (NCAs), which enables control over block sequence, block length as well as a side chain and end group functionality.[30,32–35] It is worth noting that, as a most promising PEG alternative, pSar provides comparable solution properties and stealth capability, but displays improved immunogenicity in rodents reducing accelerated blood clearance, cytokine release, and complement activation.[36–45] However, these PICMs achieve limited RNAi efficiency, which is likely due to insufficient endosomal escape.[29,46] This limitation may be abolished by the incorporation of CADs within the PICMs. But exactly such an application of CADs to foster enhanced endosomal escape in vivo was limited to LNPs (moderately improved protein expression levels) or required separate administration of CAD and nucleic acid delivery systems until now.[26] Multicompartment PICMs, which are able to encapsulate, and co-deliver siRNA and CADs at adjustable ratios have not been reported yet. Although the combination of stability and cargo protection within PICM in the blood stream as well combined with enhanced endosomal escape properties seems most promising for targeted nucleic acid delivery. In addition, such an approach reduces CAD-related systemic toxicity and allow for higher drug dosing.

In this study we introduce such systems by designing ABC-triblock polypept(o)ides namely polysarcosine-*b*-poly(γ-benzyl-L-glutamate)-*b*-poly(L-lysine) (pSar-*b*-pGlu(OBn)-*b*-pLys) copolymer, which combine a pLys block for siRNA complexation, a pGlu(OBn) block for stabilization as well as drug encapsulation by π–π interactions and a shielding pSar block for providing stealth-like properties. We use these polymers to prepare siRNA-based PICMs by dual centrifugation (DC) and evaluate the therapeutic efficiency of this novel nucleic acid delivery system in a clinically relevant HCC mouse model by targeting MFAP-5 with RNAi (**Figure 1**).[47]

2. Results and Discussion

2.1. From the pSar-*b*-pGlu(OBn)-*b*-pLys ABC-Triblock Copolymer Synthesis to siRNA PICMs

Polypept(o)ides are synthetically accessible by nucleophilic ring-opening polymerization (ROP) of *N*-carboxyanhydrides (NCAs), allowing for precise control over block length, sequence, and end group integrity under optimized conditions.[30,32,34,35,48] Herein, a simple aliphatic amine, neopentylamine, was utilized as an initiator for sequential polymerization of Sar-, Glu(OBn)- and Lys(Boc)-NCA, respectively. The successful chain extension upon sequential monomer addition is visualized in Gel Permeation Chromatography (GPC, in HFIP) elugrams by shifts of the peak

H. Zhang, L. Simic, Z. Dai, D. Schwiertz, G. Schäfer, M. Barz
Division of BioTherapeutics
Leiden Academic Centre for Drug Research (LACDR)
Leiden University
Leiden 2333CC, Netherlands
E-mail: h.zhang@lacdr.leidenuniv.nl

B. Schrörs, Ö. Akilli-Öztürk, F. Durak, M. Diken
Biosampling Unit
TRON gGmbH - Translational Oncology at the University Medical Center of the Johannes Gutenberg University
Freiligrathstr. 12, 55131 Mainz, Germany

J. Lin, K. Koynov
Max Planck Institute for Polymer Research, Physics at Interphases
Ackermannweg 10, 55128 Mainz, Germany

B. Bogaert, K. Raemdonck
Ghent Research Group on Nanomedicines
Laboratory of General Biochemistry and Physical Pharmacy
Faculty of Pharmaceutical Sciences
Ghent University
Ghent 9000, Belgium

J. M. Schattenberg, L. Kaps
Department of Medicine II
Saarland University Medical Center
Saarland University
66421 Homburg, Germany

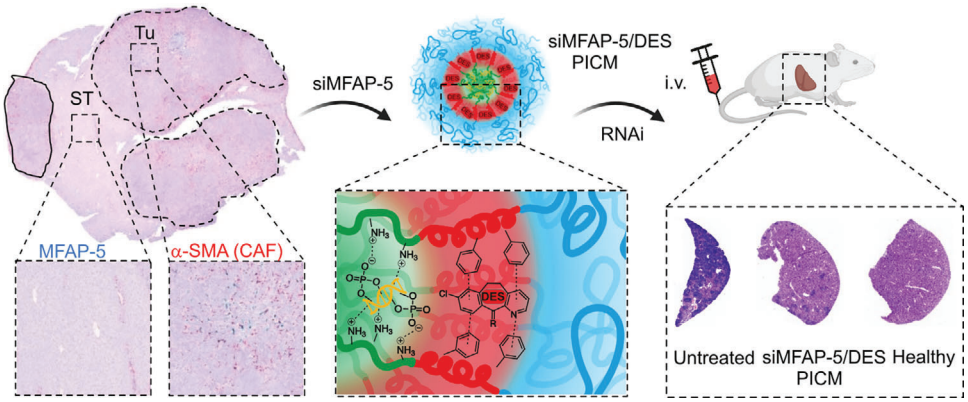

Figure 1. Schematic overview of the study – identification of MFAP-5 as a novel target in hepatocellular carcinoma (HCC) and a novel delivery system, namely PICMs for co-encapsulation of cationic amphiphilic drug desloratatine (DES) and siRNA, for the in vivo knockdown of MFAP-5 as antistromal therapy in HCC.

maximum toward lower elution volumes (**Figure 2B**), which indicates an increase in the hydrodynamic volume corresponding to an increase in molecular weight. Further, steady Poisson-like molecular weight distributions confirm controlled polymerization and the absenced of side reactions. The slight peak broadening in the final triblock copolymers is, in all probability, attributed to the presence of secondary structures in the peptide segments, which is known to determine hydrodynamic volume and solution properties.[49] Indeed, the observed shifts in elution volume due to chain ectension are rather small, which is attributed to the minor chain length of pGlu(OBn) and pLys(Boc) in comparison to the first block of pSar. The structural integrity of the ABC-triblock copolymers was demonstrated by ^{1}H diffusion-ordered spectroscopy (DOSY) NMR, assigning all proton species of the different blocks to a single diffusing species (Figure 2C). The chain length of different blocks was determined by end-group analysis in ^{1}H NMR (Figure S1A, Supporting Information). Normalized on the integral of distinct initiator end group signal at 0.84 ppm, the chain length of pGlu(OBn) was determined by the integrals of the benzyl signal at 4.92–5.07 ppm and 7.36–7.19 ppm ($X_{n,pGlu} = 12$). Chain length of pLys(Boc) was determined by the integral of Lys-N$_\epsilon$HCO-signal at 6.66 ppm ($X_{n,pLys} = 8$) and pSar length by integrals of CH_2- and CH_3-related signals (2.72–2.96 ppm and 3.89–4.38 ppm; $X_{n,pSar} = 190$), subtracting underlying values of previous analyzed blocks. Further, the chain length of pSar as the first block was verified by HFIP GPC and external calibration with pSar standards.[50] Subsequently, the Boc-protective groups on the pLys segment were removed by TFA/H_2O (v/v 1:1), as displayed in Figure 2A, yielding free primary amine groups that can complex anionic nucleic acids (e.g., siRNA) by electrostatic interaction upon protonation.[51] The deprotection was confirmed by ^{1}H NMR (Figure S1B, Supporting Information), displaying complete loss of the Boc-signal at 1.35 ppm and NεHCO-signal at 6.66 ppm as well as gain of a broad amine signal. Resistance of the polymeric backbone against deprotection conditions is ensured by HFIP GPC (Figure S1C, Supporting Information). The observed minor alteration in the elugram derives from interactions of liberated amine functional groups with the column material. Moreover, we synthesized a similar ABC-triblock copolymer with an inverse synthetic route, demonstrating the versatility of the chemical approach to design such type of material (Figure S2A, Supporting Information). NMR analysis confirmed the polymeric structure and chain lengths of (Neo)pLys$_{12}$-*b*-pGlu(OBn)$_{17}$-*b*-pSar$_{239}$(N$_3$) (Figure S2B,C, Supporting Information).[59] Notably, this synthetic approach provides the possibility to functionalize the pSar chain end and thus modify the outside of resulting PICMs by reactive-ester chemistry with an azide functionality to open the window for bioconjugation by click-chemistry, either targeting moieties for active targeting or markers for visualization and tracking of particles.[52–56]

Both triblock copolymers displayed the best compromise between solubility in aqueous solution, and encapsulation efficiency (drug and siRNA), while longer pGlu(OBn) blocks caused aggregation in aqueous solution and longer pLys blocks did not improve encapsulation efficacy nor serums stability while shorter ones failed to encapsulate siRNA efficiently. Thus, those systems were discarded for further studies. With the optimal triblock copolymer of (Neo)pSar$_{190}$-*b*-pGlu(OBn)$_{12}$-*b*-pLys$_8$, a full complexation of siRNA was observed at N/P ratio 3 (Figure S3B, Supporting Information), before siRNA containing PICM have been fabricated by dual centrifugation to enable drug and siRNA loading in a single step.

The previous work and additional screening in this project have demonstrated that lysine-based PICMs are not efficient in delivering siRNA into the cytosol of target cells, underlining that endosomal escape remains the major obstacle for such systems (**Figure 3A**).[29] We screened various CADs, including desloratadine (DES), nortriptyline (NOR), and loperamide (LOP) to foster endosomal escape (Figure S3C, Supporting Information). Those different CADs were incorporated into PICMs to cause lysosomal membrane permeabilization and therefore enable entrance of siRNA into the cytosol of cells.[58–61] First, we screened varying concentrations (20, 40, and 60 µM per well) using H1299 epithelial-like cells that stably express green fluorescent protein (GFP) (H1299_GFP) with respect to silencing efficiency (displayed as relative mean fluorescence intensity of GFP based on non-treated cells, GFP rMFI), according to the protocol from previous report (Figure S3D, Supporting Information).[62] However, there was limited improvement in GFP silencing, regardless of concentration and CAD type. Extending the exposure time of cells to siRNA PICMs from 4 to 24 h, however, increased

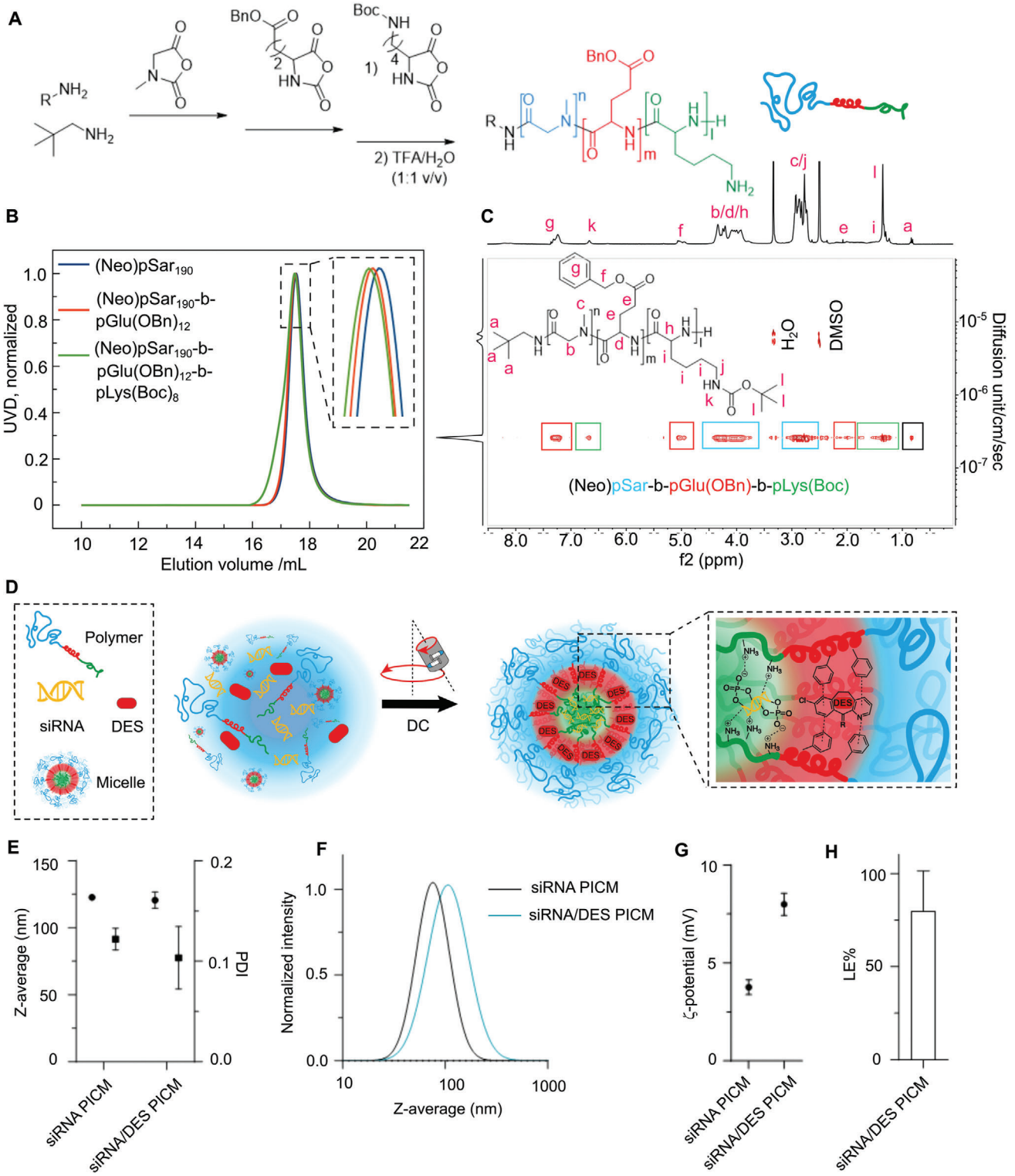

Figure 2. ABC-triblock polypept(o)ide synthesis, characterization and formulation. A) Synthetic route to derive (Neo)pSar-*b*-pGlu(OBn)-*b*-pLys synthesis by amine-initiated sequential ROP of respective NCAs and subsequent Boc-deprotection. Characterization of (Neo)pSar-*b*-pGlu(OBn)-*b*-pLys(Boc) by B) GPC in HFIP and C) ^{1}H DOSY NMR in DMSO displaying chain growth, monomodal size distribution in each polymerization step and structural integrity. D) Scheme of siRNA/DES PICMs formation by DC and siRNA/DES arrangement within the PICM compartments by electrostatic (siRNA) and hydrophobic/π-π (DES) interaction. E–G) Size, size distribution, and ζ-potential of siRNA PICMs and siRNA/DES PICMs in HEPES buffer (10 mM, pH7.4) measured by dynamic light scattering (DLS). H) Loading efficiency of DES within siRNA/DES PICMs was quantified by ultra-performance liquid chromatography (UPLC).

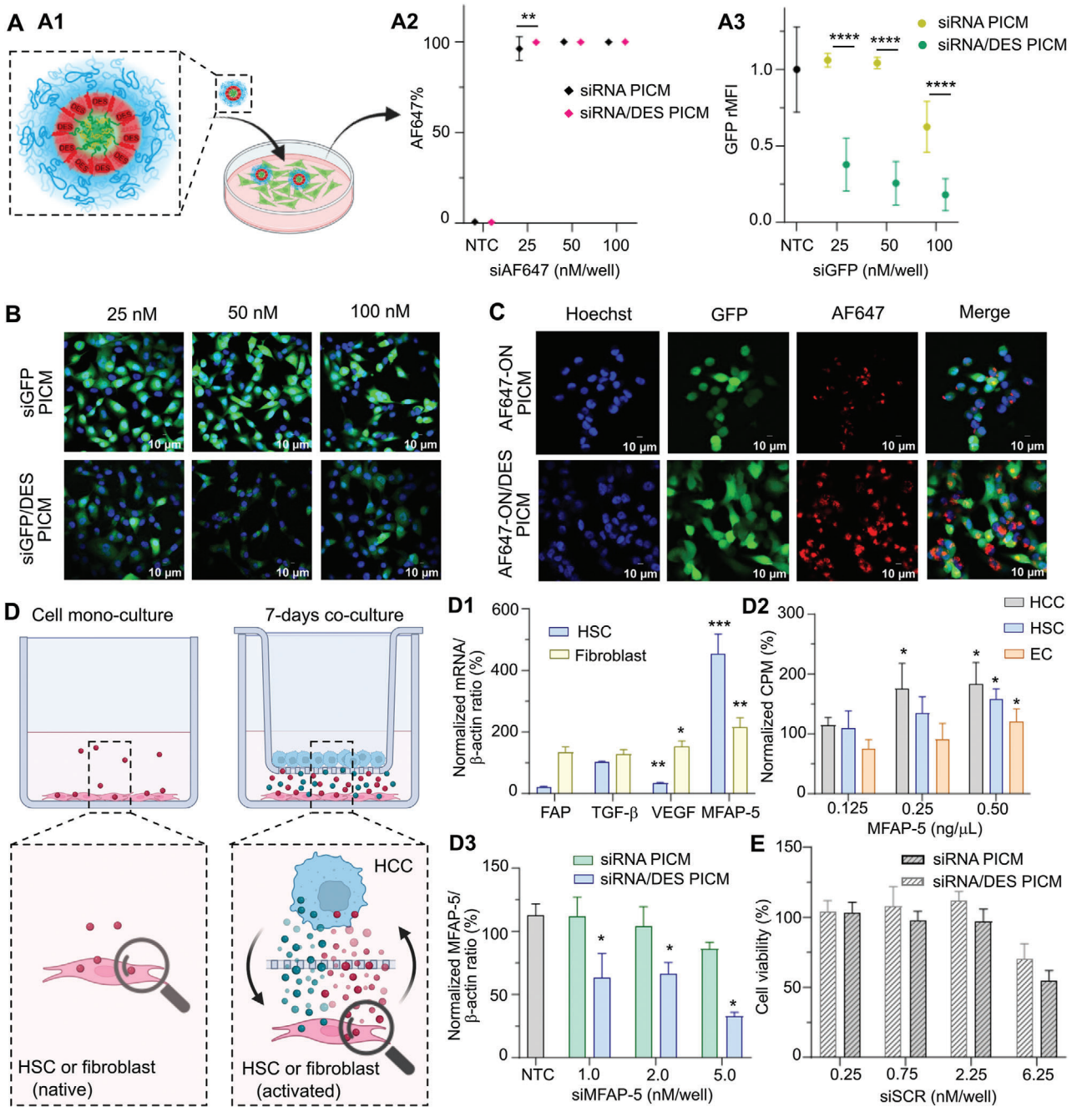

Figure 3. In vitro biological performance of siRNA PICMs and siRNA/DES PICMs. A1) In vitro evaluation of siRNA PICMs and siRNA/DES PICMs on H1299 cells that stably express green fluorescence protein (H1299_GFP cells). A2) H1299_GFP cells were exposed to AF647-labeled scrambled siRNA (siAF647) PICMs or siAF647/DES PICMs for 24 h before flow cytometry measurements. A3) In vitro knockdown of GFP in H1299_GFP cells. Cells were exposed to anti-GFP siRNA (siGFP) PICMs or siGFP/DES PICMs for 48 h before flow cytometry measurements, as represented by GFP rMFI compared to non-treated cells (NTC). B) Representative confocal images of GFP knockdown in H1299_GFP cells after being exposed to siGFP PICMs and siGFP/DES PICMs for 48 h at varying doses of siGFP (scale bar: 10 μM). C) Evaluation of increased endosomal escape by confocal microscopy images of H1299_GFP cells (green: GFP, blue: nuclei by hoechst staining) upon 24 hours' incubation with AF647-labeled oligonucleotides (AF647-ON) PICMs or AF647-ON/DES PICMs (red) with final concentrations of 50 nM AF647-ON/40 μM DES in each well by confocal microscopy (scale bar: 10 μM). D) Schematic illustration of the co-culture activation of CAF precursor cells (hepatic stellate cells (HSC), 3T3-fibroblasts) with hepatocellular carcinoma (HCC) cells (Dt81Hepa1-6). D1) RT-qPCR analysis of activated HSC or 3T3-fibroblasts following co-culture activation. MFAP-5 was highly upregulated. D2) When incubated with increasing concentrations of recombinant MFAP-5, HCC cells, HSC, and EC showed dosage-dependent increase of proliferation as determined by ^{3}H-Thymidine counts per minute (CPM). D3) siMFAP-5/DES PICMs were able to efficiently knockdown MFAP-5 in co-culture activated HSC, while siMFAP-5 PICMs were not effective. Gene expression was normalized to non-treated cells (NTC). E) Cell viability of scrambled siRNA (siSCR) PICMs and siSCR/DES PICMs was assessed on HSC (MHSC-SV40) by an MTT assay. Statistical analysis was performed by 2-way ANOVA with the software GraphPad Prism 10 (*$p < 0.05$, **$p < 0.01$, ***$p < 0.001$, ****$p < 0.0001$).

GFP silencing in a dose-dependent pattern for LOP (up to 10%), and even more dominant for DES, ranging from 21% to 54%, whereas no enhancement of siRNA-mediated GFP suppression was observed for NOR at all tested doses (Figure S3E, Supporting Information). Further, we simultaneously applied DES (with final concentration of 20 and 40 μM per well) and anti-GFP siRNA (siGFP) PICMs (with final concentration of 50 nM siGFP per well) to the cells for 24 h and observed modest GFP suppression, ≈12% and 28% at DES of 20 and 40 μM, respectively (Figure S3, F1, Supporting Information), indicating the importance of co-administration of siRNA and DES. After 48 hours' exposure, a notable decrease in GFP rMFI was found at all doses applied (*$p = 0.0220$ for 25 nM; ***$p = 0.0002$ for 50 nM; ****$p < 0.0001$ for 100 nM). The silencing effect is siGFP dose-dependent, where a reduction of 22%, 37%, and 62% in GFP rMFI was detected at a dose of siGFP 25, 50, and 100 nM, respectively. It is clear that the combination with DES enhances the GFP knockdown effect on H1299_GFP cells (Figure 3, A3; Figure S3, F2, Supporting Information). In summary, the GFP silencing efficiency was improved when DES was combined with siGFP PICMs. Moreover, increasing either the exposure time, DES dose, or siGFP dose, led to a more robust GFP knockdown.

2.2. Co-Administration of Desloratadine to Enhance In Vitro Silencing Efficiency of siRNA PICM

Due to the hydrophobic nature and aromatic moieties of both pGlu(OBn) and DES for π–π interaction, co-encapsulation of DES and siRNA is feasible and can be easily achieved by utilizing the DAC approach for kinetically enforced phase separation and PICMs formation (i.e., siRNA/DES PICMs), as displayed in Figure 2D. As stated before, compared to siRNA PICMs, siRNA/DES PICMs displayed a comparable size ≈120.6 ± 6.1 nm (PDI 0.103 ± 0.0311) (Figure 2E). Alteration of hydrodynamic radii toward bigger values can be expected upon DES loading due to the swelling of hydrophobic domains in the core of PICMs. The monomodal size distribution and the PICMs-mediated solubility of DES in aqueous solution indicate the formation of PICMs co-loaded with DES and siRNA (Figure 2F). The surface charge (ζ-potential) of PICMs remained neutral when DES was co-loaded. The value is comparable to siRNA PICMs (3.8 ± 0.38 mV vs 8.0 ± 0.57 mV) (Figure 2G). A drug loading efficiency of 85.4% was determined using ultra-performance liquid chromatography (UPLC) (Figure 2H). Moreover, the presence of DES did not affect siRNA complexation and quantification (Figure S3G,H, Supporting Information). Further, both siRNA PICMs and siRNA/DES PICMs did not show any siRNA leakage nor aggregation in full human serum in fluorescence correlation spectroscopy studies, which is in line with our previous findings on PICMs employing pSar for shielding of PICMs (Figure S4, Supporting Information).[57]

Besides studying RNAi alone, cellular internalization was investigated first (Figure 3A). AF647-labeled non-targeting siRNA (siAF647)/DES PICMs were endocytosed into over 95% of cells at all siRNA concentrations. In general, the cellular internalization is not affected by co-encapsulation of DES, except at a low dose of 25 nM (**$p = 0.0071$) (Figure 3, A2). When H1299_GFP cells were exposed to siGFP/DES PICMs at final siGFP concentrations of 25, 50, and 100 nM, significant and dose-dependent GFP suppression of 62%, 74%, and 82% was observed respectively, pointing toward functional siRNA-mediated gene silencing. In a direct comparison with siRNA PICMs, a remarkable increase in GFP silencing was detected (****$p < 0.0001$) when siGFP and DES were co-encapsulated into PICMs, suggesting a benefit for DES to act in close proximity to PICMs to boost endosomal release of siRNA (Figure 3, A3). Confocal images supported the silencing effect of siGFP/DES PICMs (Figure 3B, bottom panel). To verify the contribution of DES in endosomal escape events, cells were exposed to PICMs encapsulating AF647-labeled oligonucleotide (AF647-ON) and DES and then visualized using confocal microscopy, according to the previously reported dequenching assay.[63,64] When PICMs were trapped into endosomes, AF647 fluorescence is concentrated within the vesicles and quenched, whereas an intense burst and distribution of AF647 fluorescence was observed once AF647-ON escaped from endosomal/lysosomal compartments to the cytosol of cells. This allows to visualize the endosomal escape events (Figure 3C). Especially the uniform distribution of AF647 fluorescence over the cytosol of cells taking up PICMs indicates efficient endosomal escape upon administration of AF647-ON/DES PICMs compared with AF647-ON PICMs. Thus, the increased GFP silencing efficiency, mediated by DES, is attributed to an enhanced endosomal escape, as reported before for other applications.[62]

With respect to therapeutic RNAi, we explored the antitumoral effect of siRNA-loaded PICMs targeting cancer-associated fibroblasts (CAFs) and the related MFAP-5.[65] As highly secretory cells, CAFs are key players in tumor development and contribute substantially to the nature of the TME. They produce cytokines, growth factors and promote blood vessel formation, cancer cell proliferation, migration, invasion, and therapeutic resistance.[66–68] Therefore, CAFs and CAF-related signaling represent promising targets for anticancer therapy.[69] Among these, FAP (fibroblast activation protein), TGF-β (transforming growth factor beta), VEGF (vascular endothelial growth factor) and in particular MFAP-5 are promising as these signaling molecules promote tumor growth of HCC and other solid tumors (Figure S5, Supporting Information). For instance, MFAP-5 blockage inhibited fibrosis, neoangiogenesis, and enhanced chemosensitivity in ovarian and pancreatic cancer.[70] In addition, overexpression of MFAP-5 in CAFs proved to be predictive for survival in patients with ovarian cancer.[17] MFAP-5 is also used as a diagnostic marker for the early detection of prostate cancer.[71] However, yet there is a lack of relevant (pre-)clinical data regarding the relevance of MFAP-5 in HCC (Figure S5A, Supporting Information). Thus, MFAP-5 expression in HCC was tested by an online available database analysis (TIMER), where survival rates of patients are estimated based on specific gene mutations.[72,73] Here, high expression of MFAP-5 is associated (log-rank $p = 0.03$) with poor survival in patients with HCC (Figure S5B, Supporting Information).

To establish a predictive in vitro system, hepatic stellate cells (HSC, MHSC-SV40) and fibroblasts (NIH/3T3), both reflecting precursor cells of CAF in vitro, were co-cultured with HCC cells (Dt81Hepa1-6) to induce an activated CAF-similar phenotype (Figure 3D).[47,74] MFAP-5 was highly upregulated in both activated HSC and fibroblasts (Figure 3, D1). In contrast, MFAP-5 expression was very low in the HCC cells (Figure S6, Supporting

Information). Further, recombinant MFAP-5 stimulated the cell proliferation of HCC, HSC, and EC in a dose-dependent manner (0.25 and 0.50 ng μL^{-1} MFAP-5, $^{*}p < 0.05$), suggesting a panmitogenic effect of MFAP-5 (Figure 3, D2). Next, the knockdown efficacy of siRNA-loaded PICMs was tested in vitro by examining a sequence-specific knockdown of MFAP-5 mediated by anti-MFAP-5 siRNA (siMFAP-5) in HSC that was activated before by co-culturing with HCC cells. PICMs containing both DES and siMFAP-5, reduced significantly ($^{*}p < 0.05$) MFAP-5 transcripts in HSC at low doses of siMFAP-5 (1, 2, and 5 nM) as determined by RT-qPCR (Figure 3, D3). In contrast, siRNA PICMs without DES failed to knockdown MFAP-5. Both systems were non-cytotoxic at relevant concentrations below 6.25 nM siRNA, suggesting good biocompatibility of the developed siRNA/DES PICMs (Figure 3E; Figure S7, Supporting Information). To sum up, MFAP-5 was highly upregulated in both fibroblasts and HSC, when co-cultured with HCC cells and displayed a pro-proliferative effect. Compared to siRNA PICMs, siRNA/DES PICMs led to a robust reduction of MFAP-5 expression in activated HSC.

2.3. siRNA Loaded PICMs Accumulate Efficiently in CAF of the HCC Liver Tumors

Before therapeutic experiments, in vivo, the biodistribution of siRNA-containing NPs was investigated on both organ and cellular levels in HCC-bearing mice. Therefore, an intrasplenic, syngeneic HCC injection model was chosen, which reflects the multifocal disease in patients.[47] Fluorescently labeled siRNA (Cy5.5-labeled siRNA, siCy5.5)-loaded PICMs with or without the presence of DES were intravenously injected. LNPs were utilized as reference NPs as this formulation is used for the approved liver-targeting drug Onpattro for the treatment of hereditary transthyretin-mediated amyloidosis (Figure S8, Supporting Information). In addition, mice were injected with free siCy5.5 to compare the pharmacokinetics with encapsulated siRNA. HCC-bearing mice were intravenously injected with siCy5.5 PICMs and siCy5.5/DES PICMs at day 26 after tumor cell inoculation when liver tumors were fully established. After injection, the whole-body distribution was monitored by an in vivo near-infrared (NIR) imaging system at 0, 1, 3, 6, 24, and 48 h (**Figure 4A**). First, all different siCy5.5-loaded NPs showed a comparable organ tropism and accumulated primarily in cancerous livers. At 24 h post-administration, Cy5.5 signal from siCy5.5 PICMs and siCy5.5/DES PICMs was mainly located in the liver region, while the signal of siCy5.5-loaded in LNPs began to fade and was less localized in the liver region. In the mice administrated with free siCy5.5, the fluorescence signal strongly reduced over time. At 48 h post-administration, almost no fluorescence was detectable, indicating that the majority of free siCy5.5 was cleared mostly over the urinary tract as a low fluorescence signal in the bladder region indicated (Figure 4B; Figure S9, Supporting Information). At 48 h post-administration, mice were sacrificed, and their organs were extracted for *ex vivo* imaging to quantify accurately the fluorescence signal in each organ. Mice treated with siCy5.5-loaded NPs showed a significantly higher fluorescence signal in the liver ($^{***}p < 0.001$) compared with mice treated with free siCy5.5, indicating that at least unmodified siRNA needs to be encapsulated in NPs to accumulate in high dose in the liver (Figure 4C,D). After 24 h, there was also a fluorescence signal in the kidneys, which could be observed before for other nanoparticle systems for functional siRNA delivery in hepatic myofibroblasts for liver fibrosis therapy.[75,76] Overall, the intensity of fluorescence signals in the cancerous liver was comparable between the different NPs.

Next, we quantified cell-specific uptake in vivo after enzymatic digestion of the dissected livers. The resulting single-cell suspension was subjected to flow cytometry (Figure 4E; Figure S10A, Supporting Information). While there was no uptake of free siCy5.5, siCy5.5-loaded NPs showed a robust uptake into non-parenchymal cells (CAF > dendritic cells (DC) > macrophages (Mϕ) > T-cells (TC)), while less uptake was found for tumor cells (HCC). The low uptake of the siCy5.5-loaded NPs in HCC cells may originate from the fact that the tumors are encapsulated by a desmoplastic stroma which protects them from invasion of immune cells or also smaller objects like NPs (Figure S11, Supporting Information), which makes antistromal therapies particularly promising for such tumors.

In a direct comparison, siRNA/DES PICMs achieved a significantly ($^{**}p < 0.01$) higher uptake into CAFs than siRNA LNPs. We hypothesize that the LNP formulation applied in this study is optimized for siRNA delivery to hepatocytes (e.g., to target transthyretin) and displays more pronounced uptake into such cells than PICMs.[77,78]

2.4. In Vivo Knockdown of MFAP-5 with siMFAP-5 Loaded PICMs for Antitumor Therapy

We decided to test a siRNA-mediated knockdown of MFAP-5 for HCC therapy for three reasons. First, MFAP-5 plays a pathomechanistic role in HCC and other solid cancers as shown by TIMER analysis as well as in literature. Second, MFAP-5 is highly upregulated in CAF-precursor cells (fibroblasts, HSC) in co-culture with HCC cells and has a panmitogenic effect on tumor-relevant liver cells in vitro. Third, siRNA-containing PICMs transport siRNA efficiently into HCC livers and are predominantly taken up by CAFs, even in the absence of active targeting.

For in vivo knockdown, PICMs containing anti-MFAP-5 siRNA (siMFAP-5) alone or siMFAP-5 and DES were administered intravenously at 0.5 mg kg^{-1} (low dose) or 1.0 mg kg^{-1} siMFAP-5 (high dose), respectively to HCC mice on day 21, 23, and 25 post-tumor cell inoculation. On day 28, mice were sacrificed, and organs and blood were harvested for analysis (**Figure 5A**). As tumor nodules were multinodular and confluent, rendering quantification of individual nodules by counting unreliable, liver weights were assessed as surrogate markers for tumor load. This data was correlated with *ex vivo* tissue sections which were stained with hematoxylin and eosin (H&E) and analyzed by microscopy. Mice treated with siMFAP-5/DES PICMs at a high dose of siMFAP-5 had significantly ($^{***}p < 0.001$) lower liver weights than controls (non-treated controls (NTC)), indicating reduced tumor burden (Figure 5B). As a second readout to quantify tumor load, we have quantified alpha-1-fetoprotein (AFP) in the sera of mice. AFP is an established tumor marker for HCC in the clinical diagnostic and shows a good correlation

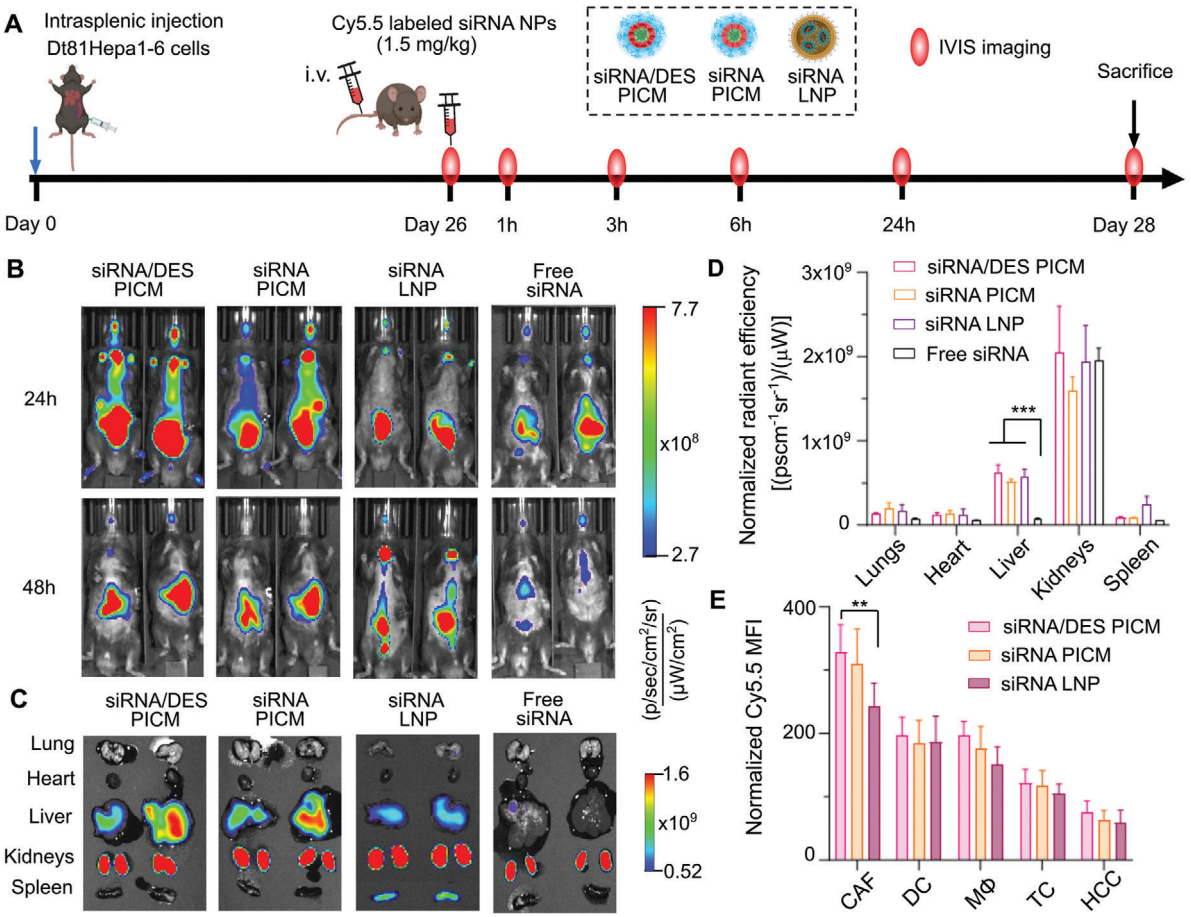

Figure 4. In vivo biodistribution of Cy5.5-labeled scrambled siRNA (siCy5.5)-loaded nanoparticles (NPs) in mice with hepatocellular carcinoma (HCC). A) Intrasplenic injection of HCC cells (Dt81Hepa1-6) to develop tumors in the livers. On day 26 post-tumor cell inoculation, HCC mice were intravenously injected with siCy5.5 PICMs, siCy5.5/DES PICMs or siCy5.5 LNPs (corresponding to 1.5 mg kg^{-1} siRNA). Biodistribution of the NPs was monitored by a NIR-imaging system at 0, 1, 3, 6, 24, and 48 h. B) In vivo biodistribution of the siCy5.5 NPs at 24 and 48 h. C) Ex vivo imaging of extracted organs at 48 h post-administration. D) Quantification of organ fluorescence of the extracted organs shown in C). E) In vivo cellular uptake of siCy5.5 NPs in liver cells (CAF, cancer-associated fibroblasts; DC, dendritic cells; Mϕ, macrophages; TC, T-cells; HCC, hepatocellular carcinoma cells), as quantified by flow cytometry of liver single-cell suspension obtained from enzymatically digested livers shown in C). Statistical analysis was performed by *t*-test with the software GraphPad Prism 10 ($n = 2$–5, $^{**}p < 0.01$, $^{***}p < 0.001$).

($r^2 = 0.83$) with the tumor load in our model (Figure S12, Supporting Information). In line with the reduction of liver weights, AFP sera levels were significantly lower in mice treated with siRNA/DES PICMs, at both low ($^{****}p < 0.0001$) and high doses ($^{***}p < 0.001$). There was also a significant reduction in AFP sera levels in the mice treated with high-dose siMFAP-5 PICMs ($^{**}p < 0.01$), suggesting that AFP may be a more sensitive quantitative readout for the tumor load than biometric parameters. Interestingly, no antitumor effect was observed in mice treated with neither low nor high doses of siMFAP-5 LNPs (Figure 5C). As a third quantitative assessment of tumor burden, histological liver sections were analyzed. In H&E stained liver sections, tumor load can be morphometrically quantified by microscopy as nodules have more contrast than healthy tissue (Figure 5G; Figure S13, Supporting Information). Morphometric analysis confirmed that tumor load was significantly reduced in mice treated with low ($^{**}p < 0.01$) and high dose ($^{****}p < 0.0001$) siRNA/DES PICMs, which is confirmative to the AFP tumor marker levels. Again, LNP and PICM formulations without co-encapsulated DES showed no significant reduction in tumor load (Figure 5D).

Next, we tested whether siRNA-mediated knockdown of MFAP-5 may correlate with the antitumor effect in the mice to rule out an unspecific effect of the nanoparticular treatment. A significant knockdown for MFAP-5 was achieved in all siMFAP-5 treated mice but with different efficacy. Of note, the strongest MFAP-5 reduction (60% reduction vs NTC and even down to levels of healthy control mice) was found in the high dose siMFAP-5/DES PICMs treated mice, which also showed the best antitumor response (Figure 5E). This knockdown pattern could also be observed on the protein level as assessed by FACS analysis of all liver cells (Figure 5F).

To test the toxicity of all formulations, repetitive dosing of overdosed siRNA loaded NPs (corresponding up to 3.0 mg kg^{-1} siRNA) was well-tolerated by healthy mice and no acute toxicity could be observed by abnormal behavior, macroscopic inspection of the organs and safety laboratory parameters (e.g., hemolysis, acute liver and kidney damage). Moreover, analysis of

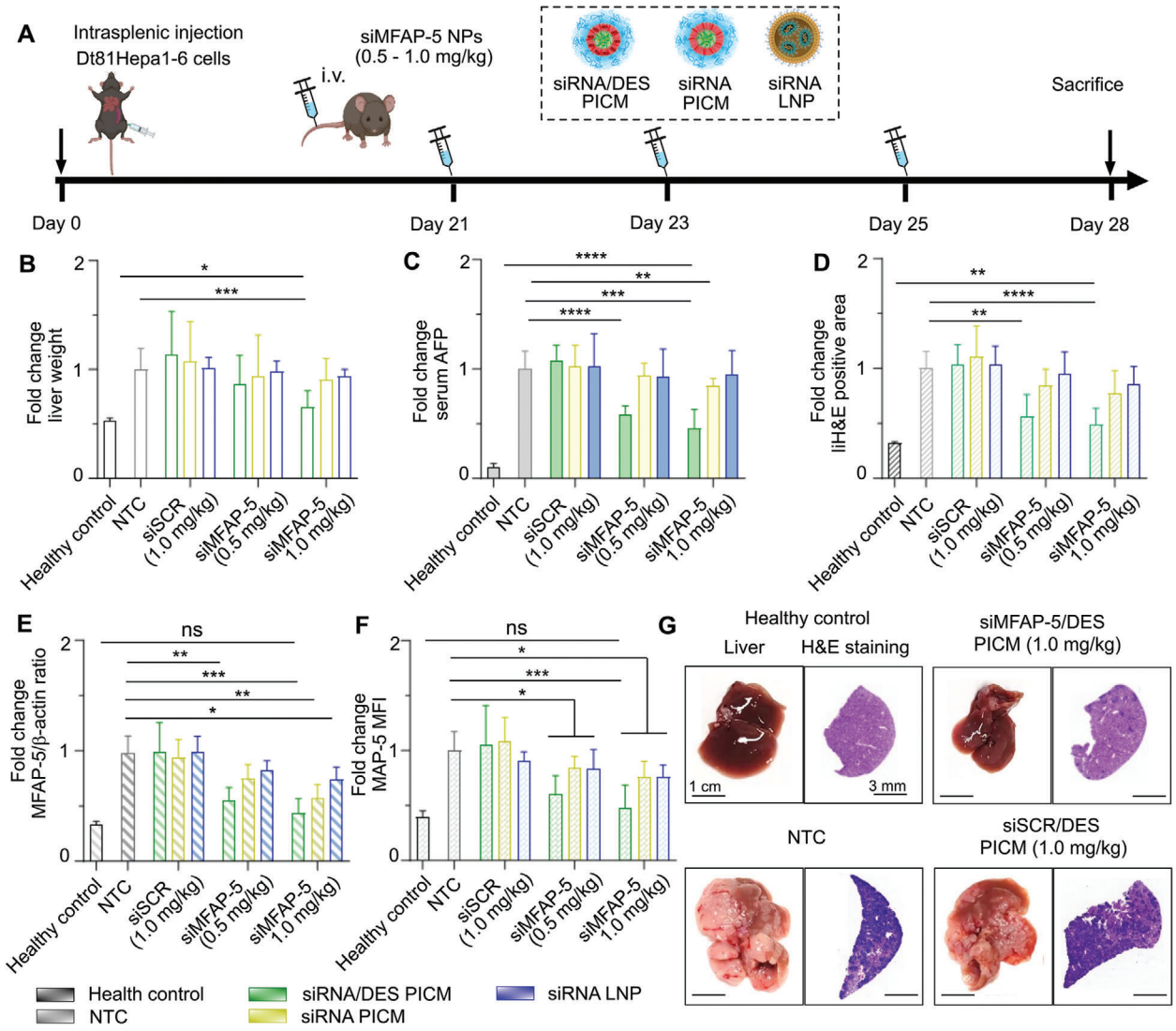

Figure 5. In vivo knockdown with anti-MFAP-5 siRNA (siMFAP-5)loaded nanoparticles (NPs) in HCC-bearing mice ($n = 5$ in each group). A) HCC cells (Dt81Hepa 1–6) were intrasplenically injected into mice to induce tumors exclusively in their livers. Tumor-bearing mice were intravenously injected with siMFAP-5 PICMs, siMFAP-5/DES PICMs or siMFAP-5 LNPs (all corresponding to 0.5 or 1.0 mg kg^{-1} siMFAP-5) on day 21, 23, and 25 post-HCC cells' inoculation, while controls received 1.0 mg kg^{-1} encapsulated scrambled siRNA (siSCR) or equal volumes of PBS (non-treated control, NTC). On day 28, mice were sacrificed and B) livers were weighed and C) serum alpha-fetoprotein (AFP) levels of mice were quantified by ELISA. D) Tumor load was morphometrically determined in H&E-stained liver sections. Quantification of MFAP-5 knockdown on E) mRNA level by RT-qPCR and F) protein level by flow cytometry in siRNA- and PBS-treated mice. G) Representative livers from treated, non-treated and healthy mice at sacrifice and corresponding H&E microscopic images of liver sections (Figure S13, Supporting Information) (*$p < 0.05$, **$p < 0.01$, ***$p < 0.001$, ****$p < 0.0001$ vs non-treated control (NTC) mice).

inflammatory cytokines suggested the absence of immune activation of the treatment as inflammatory cytokine levels (e.g., IFN-α, IFN-β) remained below detectable limits (Figure S14, Supporting Information).

In conclusion, siMFAP-5/DES co-loaded PICMs yielded a convincing antitumor effect at 1.0 mg kg^{-1} anti-MFAP-5 siRNA, while PICMs without DES and LNPs did not show a significant therapeutic effect, likely due to the fact that LNP are designed for hepatocyte targeting or PICMs without DES do not induce efficient endosomal escape of the loaded siRNA. Further analysis was warranted to explore the mechanistic effect of the MFAP-5 knockdown.

2.5. MFAP-5 Knockdown in CAFs Reduces Tumor Angiogenesis

In line with the literature, in vitro data indicated that CAFs might be the primary source for MFAP-5 in HCC. We analyzed histologically the TME of HCC mice to locate the cells of origin for MFAP-5. In RNAscope analysis, MFAP-5 expression co-localized with cells expressing alpha-smooth muscle actin (α-SMA), an established marker for CAF.[79] Interestingly, MFAP-5 was only found in the tumor and the TME (in proximity to tumor nodules) and was absent in the healthy surrounding tissue (**Figure 6A**). Next, we sought to clarify the pathomechanism of MFAP-5 in the HCC model. CD34 is a monomeric transmembrane

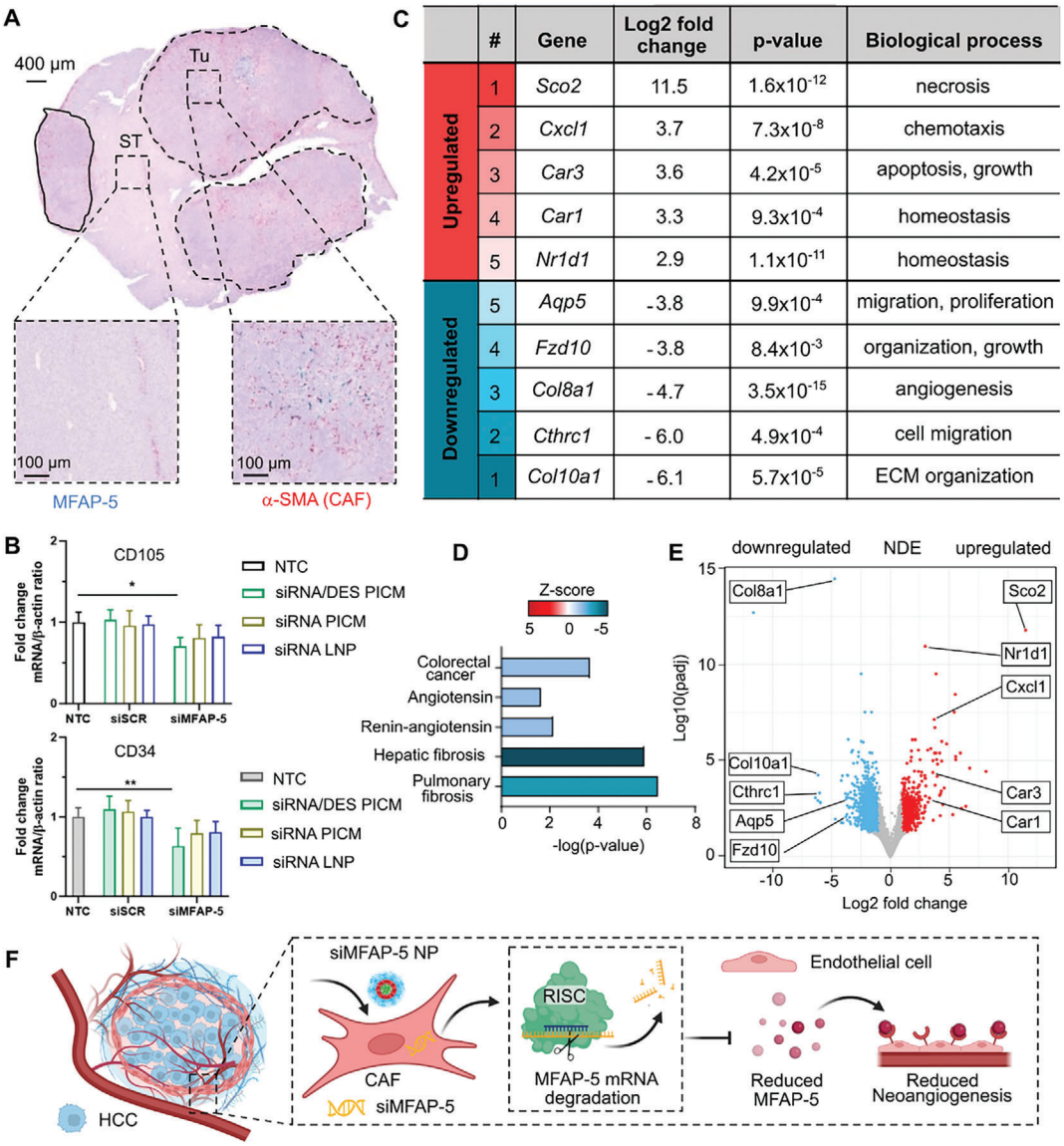

	#	Gene	Log2 fold change	p-value	Biological process
Upregulated	1	*Sco2*	11.5	1.6×10^{-12}	necrosis
	2	*Cxcl1*	3.7	7.3×10^{-8}	chemotaxis
	3	*Car3*	3.6	4.2×10^{-5}	apoptosis, growth
	4	*Car1*	3.3	9.3×10^{-4}	homeostasis
	5	*Nr1d1*	2.9	1.1×10^{-11}	homeostasis
Downregulated	5	*Aqp5*	-3.8	9.9×10^{-4}	migration, proliferation
	4	*Fzd10*	-3.8	8.4×10^{-3}	organization, growth
	3	*Col8a1*	-4.7	3.5×10^{-15}	angiogenesis
	2	*Cthrc1*	-6.0	4.9×10^{-4}	cell migration
	1	*Col10a1*	-6.1	5.7×10^{-5}	ECM organization

Figure 6. Knockdown of MFAP-5 in cancer-associated fibroblasts (CAF) reduced tumor angiogenesis and deregulated key transcripts, which are found in pathways related to angiogenesis, tumors, and hepatic fibrosis. A) Expression of MFAP-5 colocalized with CAFs (α-SMA+) in the tumor microenvironment (TME), while no MFAP-5 expression was detected in surrounding healthy tissue as determined by histological analysis of liver sections with RNAscope. B) Transcripts of the angiogenesis markers CD105 and CD34 were reduced in the livers of HCC mice treated with siMFAP-5/DES PICMs compared to controls ($*p < 0.05$,$**p < 0.01$ vs NTC). C) Top 5 relevant up- and down-regulated genes as determined by RNA-seq of representative liver samples from siMFAP-5/DES PICM versus siSCR/DES PICMs treated HCC mice (each $n = 3$, p values adjusted for multiple testing by the Benjamini-Hochberg method). D) Relevant tumor angiogenesis, fibrosis or cancer signaling pathways, which were found to be downregulated as predicted by Ingenuity pathway analysis (IPA) based on the RNA-seq differential expression data (bars represent p values adjusted for multiple testing by the Benjamini–Hochberg method, color-code represents up-(red) or downregulation (blue)). E) Volcano plot and numbers of significantly differentially expressed genes between siMFAP-5/DES PICMs versus siSCR/DES PICMs. Differentially expressed genes with log2-fold change > 1 or <1 and FDR < 0.05 are shown in red (upregulated) or blue (downregulated), respectively. Non-differentially expressed genes (NDE) are shown in grey. The top 5 relevant up- and down-regulated genes are labeled. F) siMFAP-5 loaded PICMs induce MFAP-5 RNAi to stop protein secretion from CAF. Absence of MFAP-5 reduces EC-mediated neoangiogenesis.

glycoprotein and an endothelial marker, which is restricted to a few periportal vessels in the healthy liver. In contrast, the sinusoid-like vasculature in HCC shows strong expression of CD34, which is attributed to a phenotypical change of ECs (also called capillarization of sinusoids) due to arterialized blood supply.[80] Similar to CD34, CD105 (also called endoglin) is a homodimeric transmembrane glycoprotein and is essentially expressed on ECs. An increase in CD105 occurs during various pathological processes (e.g., cardiovascular disease and tumor angiogenesis).[81] Unlike CD34, CD105 is weakly or not at all expressed in HCC tissue, giving superiority of CD34 as a marker for tumor angiogenesis (Figure S15, Supporting Information). To test for an antiangiogenic effect, the expression of the tumor-relevant angiogenesis markers CD34 and CD105 was

quantified in the livers of HCC mice, which were treated with high doses of siMFAP-5 loaded NPs and control groups (NTC, siSCR NPs). In the mice treated with high doses of siMFAP-5/DES PICMs, both angiogenesis markers CD34 and CD105 were significantly ($^*p < 0.05$) downregulated, while no changes of these transcripts were determined in control mice, revealing that MFAP-5 knockdown has inhibited tumor-related neoangiogenesis (Figure 6B,F).

2.6. Comparative Transcriptomic Analyses Detected Deregulated Key Genes Found in Angiogenesis and Tumor-Related Pathways

Comparative high-throughput RNA sequencing (RNA-seq) was applied to gain further mechanistic insight into the siMFAP-5-mediated antitumor effect. Whole liver samples of mice treated with PICMs containing DES and siMFAP-5 or siSCR ($n = 3$ each) were analyzed to reveal differences on the transcriptional level between the two groups. Among the top 5 of relevant upregulated genes, necrosis-related *Sco2* and apoptosis-related *Car3* were listed, while in the top 5 of downregulated genes, *Col8a1* and *Col10a1* were found, which are involved in angiogenesis and extracellular matrix organization, suggesting that knockdown of MFAP-5 supports cell apoptosis and inhibition of angiogenesis (Figure 6C, Table S1, Supporting Information). Ingenuity pathway analysis (IPA) was performed to correlate angiogenic and tumor-related pathways with the siMFAP-5 treatment.[82,83] Based on the differential gene expression, IPA predicts the activation and deactivation of relevant signaling pathways. For example, the frizzled class receptor 10 (Fzd10) is located upstream in the colorectal cancer metastasis signaling and was found to be significantly downregulated (e.g., Fzd10 $\log_2$-fold change of -3.8) following treatment with siMFAP-5/DES PICMs (Figure 6D,E) and thus confirm the predicted deactivation of the pathway by IPA. The colorectal cancer metastasis signaling is shown in (Figure S17, Supporting Information). Likely, the downregulation of relevant pathways related to angiogenesis (e.g., angiopoietin signaling and renin-angiotensin signaling) and organ fibrosis (e.g., hepatic and pulmonary fibrosis signaling pathway) were identified by this method as well (Figure 6D; Figure S16, Supporting Information).

3. Conclusion

Despite recent improvements by immune therapies, the prognosis of patients with hepatocellular carcinoma (HCC) at the advanced stage remains poor with low response to conventional chemotherapy. Antistromal therapy might be a novel therapeutic approach to improve the outcomes of these patients. We have identified microfibrillar-associated protein-5 (MFAP-5) as a novel target for antistromal therapy in HCC by polyion complex micelles (PICMs) induced RNA interference (RNAi) in cancer-associated fibroblasts (CAF). MFAP-5 is mainly secreted by CAF and supports tumor growth and metastasis in the tumor microenvironment (TME). We have synthesized ABC-triblock polypept(o)ide polymers to generate PICMs, which can be co-loaded with small interfering RNA (siRNA) and endosome-disruptive drugs to enhance RNAi. The nanocarriers transported efficiently their cargo into the cancerous liver of HCC mice and, here, were taken up predominantly by CAFs. Repetitive doses of MFAP-5 targeting siRNA (siMFAP-5) PICMs or siMFAP-5/DES PICMs (corresponding to 1.0 mg kg^{-1} siMFAP-5) significantly reduced the disease progression (hepatic tumor burden) as indicated by reduced liver weights, alpha-fetoprotein (AFP) serum levels and histology. In contrast, siMFAP-5 PICMs and siMFAP-5 LNPs were much less effective. The siRNA therapy was well-tolerated by the mice and no acute toxicity or adverse immune reactions could be observed. Transcriptome and detailed histological analysis revealed that knockdown of MFAP-5 reduced tumor progression as key transcripts for angiogenesis were down- and, in contrast, for apoptosis upregulated. Thus, we present an antistromal therapy for HCC, targeting CAF-derived MFAP-5 in the TME and present a PICM platform able to unleash their therapeutic potential. The non-toxic siMFAP-5/DES PICMs showed a convincing antitumor effect by interfering with the neoangiogenesis of the tumor that depends heavily on neo-angiogenesis. This therapy holds promise to treat also other solid tumors, which depend on high vascularization.

4. Experimental Section

Materials and Instruments: Unless otherwise stated, chemicals were obtained from commercial sources, such as Sigma Aldrich (Taufkirchen, Germany), TCI Chemicals (Tokyo, Japan), and Fluorochem (Hadfield, UK), used as received. *N*, *N*-Dimethylformamide (DMF) (99.8%, extra dry, over molecular sieve) was purchased from ACROS ORGANICS (Geel, Belgium), handled under light and oxygen exclusion, and purified by multiple freeze–pump–thaw cycles prior to use. Neopentylamine was dried by stirring three days with potassium hydroxide, distillation into a predried schlenk tube equipped with a molecular sieve, and stored under light und oxygen exclusion at −20 °C. Water content was verified to be lower than 50 ppm (w/w) by Karl–Fisher titration setup 899 coulometer from Metrohm (Filderstadt, Germany). NCA polymerization progress was evaluated and monitored by attenuated total reflectance Fourier transformed infrared spectroscopy, correlating monomer consumption to NCA-carbonyl bands at 1853 and 1786 cm^{-1}. Measurements were performed on an FT/IR-4100 (JASCO), equipped with an ATR sampling accessory (MIRacleTM, Pike Technologies, Madison, Wisconsin, USA) at ambient temperature. Spectra were visualized and analyzed by Spectra Manager 2.0 software (JASCO). ^{1}H NMR spectroscopy, including DOSY experiments, were carried out on a Bruker Avance I (AV-500 MHz) at ambient temperature. Deuterated dimethyl sulfoxide was obtained from Deutero GmbH (Kastellaun, Germany). Spectra were analyzed utilizing MestReNova software (version 12.0.2) with calibration by the solvent signal.[84] Gel permeation chromatography (GPC) was carried out at 40 °C with a flow rate of 1 mL min^{-1} using hexafluoroisopropanol as eluent containing 3 g L^{-1} potassium trifluoroacetate and toluene as internal standard. Hexafluoroisopropanol and potassium trifluoroacetate were purchased from Fluorochem (Hadfield, UK). The column setup with modified silica gel as column material (PFG columns, particle size 7 µM, porosity: 100 Å + 1000 Å), and PSS WinGPC software to monitor and evaluate elution diagrams, were purchased from PSS Polymer Standards Service GmbH (Mainz, Germany). Lyophilization was performed on a VirTis BenchTop Pro Freeze Dryer from SP Scientific Products. Millipore water was collected from a MILLI-Q A+ system with a resistivity of 18.2 MΩcm^{-1} and organic carbon of <5 ppb. Dynamic Light Scattering was carried out on Zetasizer Ultra from Malvern Panalytical equipped with a He-Ne-Laser (λ= 633 nm). Measurements were performed at ambient temperature, scattering angle of 173°, and utilizing disposable polystyrene cuvettes purchased from VWR (Darmstadt, Germany). Analysis of size and polydispersity based on the autocorrelation function was carried out by ZS-Xplore.

Distearoylphosphatidylcholine (DSPC) and 1,2-dimyristoyl-rac-glycero-3-methoxypolyethylene glycol-2000 (DMG-PEG2k) were purchased from Avanti Polar Lipids (Alabaster, AL, USA). Dilinoleylmethyl-4-dimethylaminobutyrate (DLin-MC3-DMA) was obtained from Med Chem Express (Monmouth Junction, NJ, USA). Cholesterol was ordered from Merck (Darmstadt, Germany). All lipid stocks were stored at −20 °C in lyophilized form or dissolved in ethanol for stock solution. 4-(2-hydroxyethyl)−1-piperazineethanesulfonic acid (HEPES), acetonitrile, *N*, *N*-dimethylformamide anhydrous (DMF), tris-base, ethylenediaminetetraacetic acid (EDTA) and D-(+)-glucose were purchased from Sigma-Aldrich (Zwijndrecht, The Netherlands). UltraPure agarose, bovine serum albumin, trypsin/EDTA and Dulbecco's Modified Eagle's Medium/F12 (DMEM/F12), trypan blue (0.4%), Hoechst 33342 and MTT (3-(4,5-Dimethylthiazol-2-yl)−2,5-diphenyltetrazoliumbromide) were purchased from Thermo Fisher Scientific (Landsmeer, The Netherlands). *L*-glutamine, PEN-STREP (10 000 U mL^{-1} penicillin, 10 000 U mL^{-1} streptomycin), and DPBS (without Ca^{2+} or Mg^{2+}) were bought from Lonza Bioscience (Verviers, Belgium). Fetal bovine serum was purchased from SERANA (Brandenburg, Germany). GelRed was bought from Bio-connect (Huissen, The Netherlands). Nortriptyline, desloratadine, and loperamide were kindly provided by Prof. Raemdonck (Faculty of Pharmaceutical Science, Ghent University, Belgium).

Chemically modified small interfering RNA and oligonucleotide, with corresponding gene target and sequences for the in vitro and in vivo experiments were purchased from commercial suppliers shown in the table as below.

Target	Abbreviation	Sequence (5'−3')	Label	Supplier
GFP	siGFP (21 nt)	Sense strand:- CAAGCUGACCCU-GAAGUUCTT	/	Eurogentec (Liège, Belgium)
		Antisense strand: GAACUUCAGGGU-CAGCUUGTT	/	
Non-targeting	siAF647 (21 nt)	Sense strand:- UGCGCUAC-GAUCGACGAUGTT	AF647-5′	
		Antisense strand: CAUCGUCGAUC-GUAGCGCATT		
Non-targeting	AF647 ON (PS linked)	GAACTTC-AGGGTCAGCTTGT	AF647-5'	
Non-targeting	siCy5.5	UGGUUUA-CAUGUCGACUAA	Cy5.5-5'	Eurofins (Mannheim, Germany)
Non-targeting (pooled)	siSCR	UGGUUUA-CAUGUCGACUAA	/	Horizon Discovery (Cambridge, UK)
		UGGUUUA-CAUGUCGACUAA		
		UGGUUUAC-AUGUUUUCUGA		
		UGGUUUAC-AUGUUUUCUGA		
MFAP-5 (pooled)	siMFAP	GAUCUCA-GAGCCUCGUAUA	/	
		ACCCUAA-UCUGGUGAACGA		
		GUGGAUG-AAGGAAUCGAAA		
		CGGGAUGA-GAAGUUUGCUU		

Polymer Synthesis and Formulation: Triblock polypept(o)ides were synthesized utilizing ring-opening polymerization (ROP) of *N*-carboxyanhydrides (NCAs) initiated by primary amines. NCAs derived from sarcosine (Sar), γ-benzyl-L-glutamic acid (Glu(OBn)), and N_ϵ-(tert-butoxycarbonyl)-L-lysine (Lys(Boc)), respectively, were synthesized and characterized as published previously.[30,85,86] Polymerization of NCAs was conducted in dry DMF under schlenk-conditions with a final concentration of ≈100 mg mL^{-1}.

(Neo)pSar-b-pGlu(OBn)-b-pLys Triblock Polypept(o)ide: Sar-NCA (273 mg, 2.373 mmol, 200 eq) was dissolved in 2 mL of dry DMF within a pre-dried Schlenk tube, cooled to 0 °C and stirred under light exclusion and argon atmosphere. Neopentylamine (3.20 µL, 2.38 µg, 0.028 mmol, 2 eq) was dissolved in 1 mL of dry DMF within an argon-flooded Eppi-tube, half of this stock solution was added to the NCA. Complete monomer conversion was observed by IR after 3 days. The vacuum was applied for several minutes to degas the solution. Glu(OBn)-NCA (47 mg, 0.178 mmol, 15 eq) was dissolved in 0.5 mL dry DMF, subsequently added to the solution, and kept stirring at 0 °C under light exclusion and argon atmosphere. Complete monomer conversion was observed by IR after 2 days. The vacuum was applied for several minutes to degas the solution. Lys(Boc)-NCA (48 mg, 0.178 mmol, 15 eq) was dissolved in 0.5 mL dry DMF, subsequently added to the solution and kept stirring at 0 °C. After another 2 days, complete monomer conversion was confirmed by IR. The polymer was precipitated by dropwise addition of the reaction mixture into 40 mL of diethyl ether. Centrifugation was performed 10 min at 4000 rpm and the supernatant was discarded. The procedure was repeated two times and the polymer dried under vacuum overnight to yield 175 mg of a colorless powder. ^{1}H NMR (500 MHz, DMSO-d_6) δ [ppm] = 7.36–7.19 (m, 5m$H_{(Glu)}$, -CH_2-Bn), 6.66 (s, 1l$H_{(Lys)}$, —N_ϵHCO—), 5.07–4-92 (m, 2m$H_{(Glu)}$, —CH_2—Bn), 4.38–3.89 (m, 2n$H_{(Sar)}$, —CH_2—) and (1m$H_{(Glu)}$, αCH) and (1l$H_{(Lys)}$, αCH), 2.96–2.72 (m, 3n$H_{(Sar)}$, —CH_3) and (2l$H_{(Lys)}$, —CH_2—N_ϵ), 2.18–1.99 (m, 4m$H_{(Glu)}$, —CH_2—CH_2—COO), 1.81–1.23 (m, 6lH(Lys), αCH-CH_2-CH_2-CH_2—), 1.35 (s, 9l$H_{(Lys)}$, OOC—$(CH_3)_3$), 0.84 (m, 9$H_{(Neo)}$, C—$(CH_3)_3$).

To remove the Boc-group from the pLys segment, the polymer was dissolved in 4 mL of water and stirred under ice cooling. TFA (4 mL) was added dropwise, the solution was stirred for 1.5 h at 0 °C and again 1.5 h at ambient temperature. The reaction mixture was transferred into a dialysis bag (MWCO 6–8 kDa) and dialyzed against Milli-Q water for 2 days and 10 mM acetic acid for 1 day. The polymer (119 mg) was obtained as colorless fluffy powder by lyophilization. ^{1}H NMR (500 MHz, DMSO-d_6) δ [ppm] = 7.36–7.19 (m, 5m$H_{(Glu)}$, —CH_2—Ph), 5.07–4.92 (m, 2m$H_{(Glu)}$, —CH_2—Ph), 4.38–3.89 (m, 2n$H_{(Sar)}$, —CH_2—) and (1m$H_{(Glu)}$, αCH) and (1l$H_{(Lys)}$, αCH), 2.96–2.72 (m, 3n$H_{(Sar)}$, —CH_3) and (2l$H_{(Lys)}$, —CH_2—N_ϵ), 2.18–1.99 (m, 4m$H_{(Glu)}$, —CH_2—CH_2—COO), 1.81–1.23 (m, 6lH(Lys), αCH—CH_2—CH_2—CH_2—), 0.84 (m, 9$H_{(Neo)}$, C—$(CH_3)_3$). For the inverse synthesis of the triblock polypept(o)ide, the sequence of NCA addition was just reversed. Further, an end group capping step was performed after sarcosine NCA polymerization by adding 20 eq of triethylamine and subsequently 10 eq of perfluorophenyl-4-azidobutanoate to stir overnight prior to precipitation.

siRNA Complexation: The ability of PICMs to complex siRNA was studied using 1.5% agarose gel electrophoresis. Briefly, 1.0 µL siRNA (5.0 µM) and varying volumes of triblock polypept(o)ide (Neo)pSar-*b*-pGlu(OBn)-*b*-pLys (1 mg mL^{-1} in 10 mM HEPES buffer) were mixed and vortexed for 20 s. A sample without the addition of polymeric solution was used as the positive control. After 1 h's equilibration at ambient temperature, samples were diluted to 20 µL with 10 mM HEPES buffer. Loading dye (4 µL; 6×) was transferred to each sample before loading into the gel pockets. Gel electrophoresis was performed at 100 V for 30 min. Images were analyzed by Image J software.

Preparation of siRNA PICMs: According to the defined N/P ratio of 3 (by agarose gel electrophoresis), 552 µL (Neo)pSar-*b*-pGlu(OBn)-*b*-pLys solution (1 mg mL^{-1} in 10 mM HEPES buffer) were mixed with 400 µL of siRNA solution (5 µM) and vortexed for 20 s. The solution was left for equilibration for 1 h and transferred to Amicon Centrifuge Spinfilter (MWCO 100 kDa), followed by washing with 2–3 mL HEPES buffer (10 mM, pH 7.4)

and being concentrated to a final volume of 500 µL. DLS measurements were performed from this solution.

Preparation of siRNA/DES PICMs: DES (0.25 mg; ≈800 nmol) were dissolved in 200 µL chloroform, transferred into a 0.2 mL PCR vial, and followed by solvent evaporation overnight. Ceramic beads (80–100 mg; SiLiBeads ZY 0.3–0.4 mm, purchased at Sigmund Lindner, Warmensteinach, Germany) were weighed into the tube, 10 µL of siRNA (100 µM, 1 nmol) and 27.6 µL (Neo)pSar-*b*-pGlu(OBn)-*b*-pLys solution (10 mg mL^{-1} in 10 mM HEPES buffer) were added and subsequently diluted with 10 mM HEPES buffer to a final volume of 100 µL. The mixture was vortexed and left for equilibration at least for 4 h. The solution was mixed vigorously by utilizing DAC (Zentrimix 380R, Hettich GmbH & Co. KG, Tuttlingen, Germany) for 1 h (2500 rpm, 4 °C). The solution was collected with a pipette and the beads washed with ≈100 µL HEPES buffer (10 mM) for four times to yield a final volume of 500 µL. The solution was filtered through a syringe filter (0.45 µM) and kept at 4 °C until use. For in vivo experiments, elevated concentrations and amounts were required. Therefore, 0.2 mL vials were filled with 50 µL of siRNA (100 µM, 5 nmol), 138 µL (Neo)pSar-*b*-pGlu(OBn)-*b*-pLys solution (10 mg mL^{-1} in 10 mM HEPES buffer) and 1.25 mg (4 µMol) DES and treated as described before, besides bead washing and filtration, to yield a final siRNA concentration of ≈0.35 µg µL^{-1}.

siRNA Release: PICMs containing siRNA and siRNA/DES (N/P 3) were prepared as described with the same concentration of siRNA. PICMs (20 µL) were incubated with 5 µL HEPES buffer or dextran sulfate for 30 min at room temperature. At the end of incubation, 5 µL of 50% glucose was added into samples before loading onto the 1.5% agarose gel, followed by electrophoresis at 100 V, 30 min. Images were analyzed by Image J software.

Preparation of siRNA LNPs: Lipids mixture containing DLin-MC3-DMA, DSPC, cholesterol, and DMG-PEG2k at a molar ratio of 50/10/38.5/1.5 were mixed in ethanol at a total lipid concentration of 15.7 mM. The siRNA stock solution (1.3 mg mL^{-1}) was diluted with citrate buffer (50 mM, pH4). Lipids and siRNA were rapidly mixed using the NanoAssemblr platform (NanoAssemblr, Precision Nano-Systems Inc., Vancouver, BC, Canada), with an aqueous-to-ethanol flow rate ratio of 3:1 (9 mL min^{-1} and 3 mL min^{-1}, respectively). The generated formulations were dialyzed against PBS (1×, pH7.4) overnight in Pur-A-Lyzer 12–14 kDa dialysis cassettes (Sigma-Aldrich, Zwijndrecht, The Netherlands) overnight at 4 °C. The samples were kept at 4 °C prior to use. Samples were loaded into Greiner 96-well black F-bottom chimney well plates (Greiner Bio-One GmbH, Alphen aan den Rijn, The Netherlands) for fluorescence measurement using a Tecan Spark microplate reader (Tecan, Switzerland) with excitation and emission wavelengths at 485 and 535 nm respectively, according to the protocol from the manufacturer.

Calibration Curve of DES: A series of concentrations of DES at 0, 1.95, 3.9, 7.8, 15.6, 31.25, 62.5, 125, and 250 µg mL^{-1} was prepared by diluting DES stock solution (10 mg mL^{-1}, DMF). A sample (20 µL of each) was injected into the column for detection by UPLC (Acquity TUV, Waters). After injection of a 20 µL sample on a Waters Acquity UPLC system, a gradient was run using a flow rate of 0.5 mL min^{-1}, starting with 95% MillQ water containing 0.1% TFA (A) with 5% acetonitrile containing 0.1% TFA (B). In 3 min, a linear gradient was run to 100% B and elution was kept for 2 more minutes on 100% B. At 5.1 min, the mixture was changed to the initial mixture. The chromatogram runtime was 7 min. Separation was accomplished with a Waters BEH C18 – 1.7 µM (2.1 × 50 mm) UPLC column and detection was done with an Acquity TUV detector set to a wavelength of 242 nm. The same method was used for the preparation of siRNA/DES with a w/w ratio of 18.7. The calibration curve was plotted as the area under the curve (AUC) with a concentration of DES applied.

Release Profile of DES: The formulated siRNA/DES PICMs (150 µL) were placed in dialysis bags (Pur-A-Lyzer Maxi Dialysis Kit, PURX12105) against 20 mL DPBS buffer with a pH7.4 and pH5 (adjusted by acetic acid) at 37 °C. At the defined timepoints of 10 min, 0.5, 1, 2, 4, 18, 48, and 72 h, 0.5 mL sample was taken outside of the dialysis bag, and 0.5 mL of DPBS with the same pH value was added. All these samples were taken to the UPLC with the same settings as described. With AUC, the accumulative release (%) of DES was calculated over time.

Stability of PICMs in Human Serum: The FCS experiments were performed on an LSM 880 (Carl Zeiss, Jena, Germany) setup. The excitation laser (He–Ne laser at 633 nm) was focused on the samples using a Zeiss C-Apochromat 40×/1.2 W water immersion objective. The fluorescence emission was collected with the same objective and directed to a spectral detection unit (Quasar, Carl Zeiss) after passing through a confocal pinhole. The fluorescence emission was spectrally separated by a grating element on a 32-channel array of GaAsP detectors operating in single photon counting mode. A detection range of 642–696 nm was used. For each sample, 30 µL of the solution was added to the ibidi 15 wells chamber (ibidi, Munich, Germany), then a series of 20 measurements, 10 s each, was performed at room temperature (23 °C). For experiments with human serum, the samples were incubated with human serum for 30 min at 37 °C prior to the measurement. The obtained experimental autocorrelation curves were fitted with the following analytical model function:

$$G(\tau) = 1 + \frac{1}{N}\sum_{i=1}^{m} \frac{f_i}{\left(1 + \frac{\tau}{\tau_{D,i}}\right)\cdot\sqrt{1 + \frac{\tau}{S^2\cdot\tau_{D,i}}}} \quad (1)$$

whereby N is the average number of diffusing fluorescence species in the observation volume, τ_{Di} is the diffusion time of the i-th species, f_i is the fraction of component i ($1 \le i \le m$), and S is the structure parameter, $S = z_0/r_0$, where z_0 and r_0 represent the axial and radial dimensions of the observation volume. The diffusion coefficients of the species D_i are related to the respective diffusion times τ_{Di} and the radial dimension r_0 of V_{obs} by $D_i = {r_0}^2/(4\tau_{Di})$. By inserting D_i into the Stokes–Einstein equation, $R_h = \frac{k_B\cdot T}{6\cdot\pi\cdot\eta\cdot D}$, the hydrodynamic radius of the respective fluorescent species could be calculated. Here, k_B is the Boltzmann constant, T is the temperature, and η is the viscosity of the solvent. As the value of r_0 depends on the optical setup, a calibration was performed using Alexa Fluor 647 (D = 330 µM^2 s^{-1} at 25 °C) as a reference standard with a known diffusion coefficient.

In Vitro Study—Cell Culture: Green fluorescent protein (GFP) stable expressing H1299 epithelial-like cells (H1299_GFP) (kindly provided by Prof. Raemdonck, Ghent University) were cultured in DMEM/F12 as well as Dt81Hepa1-6 HCC cells (kindly provided by the group of M. Bilodeau),[47] MHSC-SV40 hepatic stellate cells (Applied Biological Materials, Richmond, Canada) and NIH/3T3 fibroblasts (#CRL-1658, ATCC, Manassas, USA) were cultured DMEM. Media were supplemented with 10% fetal bovine serum (FBS), 2 mM L-glutamine, and 100 µg mL^{-1} penicillin/streptomycin to grow cells at 37 °C in 5% CO_2. Growth media were replaced regularly every two days and cells sub-cultured before reaching confluence. Cells were detached from the bottom of the flask with 0.25% trypsin/EDTA (Sigma Aldrich, Taufkirchen, Germany).

In Vitro Study—Cell Co-Culture: NIH/3T3 fibroblasts or MHSC-SV40 hepatic stellate cells were cultured into 12-well plates at densities of 14 000 cells per well. HCC cells (Dt81Hepa1-6) were seeded in ThinCerts with 8 µM pore size (Greiner, Frickenhausen, Germany) at densities of 6000 cells per insert and placed above in the same well. Cells were co-cultured for 5 days at 37 °C and 5% CO_2, then inserts were removed, and cells were harvested and lysed to harvest RNA for RT-qPCR analysis.

In Vitro Cellular Uptake: H1299_GFP cells were seeded in a 96-well plate (Greiner Bio-One GmbH, Alphen aan den Rijn, The Netherlands) with a density of 10 000 cells per well and incubated for 24 h. On the day of treatment, cells were rinsed with phosphate buffered saline (PBS) twice, before adding 20 µL of siAF647-loaded PICMs or siAF647/DES PICMs to the cells, giving a final siAF647 concentrations of 25, 50, and 100 nM per well. Controls received equal volumes of PBS. All the cells were cultured for 24 h at 37 °C, 5% CO_2. Afterward, cells were rinsed with PBS twice, trypsinized, and centrifuged at 500 g for 5 min. The cell pellet was then resuspended in a flow buffer (500 mL PBS, 0.1% NaN_3, 1% BSA) and subjected to flow cytometry with a Cytoflex (Beckman Coulter, Miami, FL, USA). The data was analyzed by FlowJo 10.6.1.

In Vitro GFP Silencing: H1299_GFP cells were seeded in a 96-well plate (7500 cells well^{-1}) at 37 °C, 5% CO_2 one day before treatment. Cells were rinsed twice with PBS (100 µL well^{-1}) and refilled 180 µL fresh culture

medium in each well. PICMs (20 µL) containing siGFP or siGFP/DES were applied, followed by 48 hours' incubation at 37 °C, 5% CO_2. When CADs were combined, the protocol was adjusted according to the different administration approaches. At the end of incubation, cells were rinsed with PBS twice, trypsinized, and collected by centrifugation (500 g, 5 min). The cell pellet was resuspended in a flow buffer for flow cytometry measurements on Cytoflex (Beckman Coulter, Miami, FL, USA). The data was analyzed by FlowJo 10.6.1.

Visualization of GFP Silencing In Vitro: H1299_GFP cells were seeded in a cell dish with glass-bottom (Φ35 mm, Greiner Bio-One GmbH) at a density of 105 000 cells well^{-1} and incubated for 24 h at 37 °C, 5% CO_2. Afterward, cells were rinsed with PBS twice and cultured with fresh culture medium (0.5 mL well^{-1}). PICMs (50 µL) containing siGFP or siGFP/DES were transferred into each cell dish to achieve the final siRNA concentration of 25, 50, and 100 nM. After 48 hours' incubation, cells were rinsed and fixed with 4% paraformaldehyde (PFA) for 15 min, followed by incubation with Hoechst 33 342 (1 mg mL^{-1} in fresh culture medium) for 30 min at room temperature. Now, cells were washed with PBS twice and incubated in a fresh culture medium at 4 °C until confocal imaging. Images would be captured with a Leica confocal microscope. Image analysis and processing were performed by Image J software.

Visualization of DES-Mediated Endosomal Escape of siRNA PICMs: H1299_GFP cells were seeded in a cell dish with glass-bottom (Φ35 mm, Greiner Bio-One GmbH, Alphen aan den Rijn, The Netherlands) at a density of 200 000 cells well^{-1} and incubated for 24 h (37 °C, 5% CO_2). Following, cells were rinsed with PBS twice and cultured with fresh culture medium (0.5 mL well^{-1}). AF647-ON PICMs or AF647-ON/DES PICMs (50 µL) were transferred into each cell dish with a final concentration of 50 nM and 40 µM DES if necessary. After 48 hours' incubation, cells were washed and fixed with 4% PFA for 15 min at room temperature, followed by incubation with Hoechst 33 342 (1 mg mL^{-1} in fresh culture medium) for 30 min at room temperature. Afterward, cells were washed with PBS twice and incubated in a fresh culture medium at 4 °C until confocal imaging. Images were captured with a Leica confocal microscope. Image analysis and processing were performed by Image J software.

In Vitro Knockdown of MFAP-5: MHSC cells were stimulated by co-culturing with HCC cells (Dt81Hepa1-6 cells) for 5 days as described above. The inserts were removed and the medium replaced with fresh cell culture media, which was supplemented with siMFAP-5 (/DES) PICMs in final concentrations of 1.0, 2.0, and 5.0 nM siMFAP-5 per well. Following 48 h, cells were collected by trypsinization and lysed for RNA extraction. MFAP-5 levels were quantified by RT-qPCR analysis.

Quantitative RT-PCR Analysis: RNA was isolated with Monarch Total RNA Miniprep Kits (New England Biolabs, Frankfurt a.M., Germany) from cells or homogenized liver tissue according to the manufacturer's protocol. Purified RNA (40 ng) was analyzed using the Luna Universal One-Step RT-qPCR Kit (New England Biolabs, Frankfurt a.M, Germany) according to the manufacturer's protocol. Primers are listed below and were purchased from Eurofins (Mannheim, Germany). Transcript levels of β-Actin were used as housekeeping gene to normalize gene expression.

Target	Forward 5'–3'	Reverse 3'–5'
FAP	GTCACCTGATCGGCAATTTG	TCGTAGATGTAGTATGTCGCTGT
TGF-β	GCAACATGTGGAA-CTCTACCAGAA	GACGTCAAAAGACAGCCACTCA
VEGF	TCCACCATGCCAAGTGGTC	GTCTCAATCGGACGGCAGTAG
MFAP-5	GTCTTGGCAATCAGCATCCC	CCAGATTAGGGTCGTCTGTGAAT
CD105	AGGGGTGAGGTGACGTTTAC	GTGCCATTTTGCTTGGATGC
CD34	CTGGGTAGCTCTCTGCCTGAT	TGGTAGGAACTGATGGGGATATT
β-Actin	GGCATTGTTACCAACT-GGGACGAC	CCAGAGGCATACAGGGA-CAGCACAG

In Vitro Proliferation Assay: HCC cells (Dt81Hepa1-6), hepatic stellate cells MHSC-SV40, and ECs SVEC4-10 cells were seeded in 96-well plates (Greiner, Frickenhausen, Germany) at a density of 5000 cells per well and allowed to adhere overnight. Cells were incubated at final concentrations of 0.5, 0.25, and 0.125 ng µL^{-1} recombinant murine MFAP-5 (R&D Systems, Minneapolis, USA). After 48 h, cell proliferation was assessed by ^{3}H-thymidine (5 µCi mL^{-1}, specific activity: 6.7 Ci mmol^{-1}, Amersham Biosciences, Freiburg, Germany) for 16 h as described before.[87] Prior scintillation counting, the cells were washed three times with PBS, lyzed using a MicroScint 20 (Perkin Elmer, Waltham, USA), and analyzed with a Tri-Carb2810 TR (Perkin Elmer, Waltham, USA). The cell proliferation was shown as normalized counts per minute (CPM).

In Vitro Cytotoxicity: In vitro cytotoxicity of scrambled siRNA (siSCR) PICMs and siSCR/DES PICMs was assessed in MHSC-SV40 murine hepatic stellate cells and Dt81Hepa1-6 HCC cells by MTT assay. In brief, MHSC-SV40 and Dt81Hepa1-6 cells were seeded in96-well plates (Greiner, Frickenhausen, Germany) at a density of 5000 cells per well and incubated in 200 µL of appropriate growth medium. Following adhesion of the cells over-night, increasing concentrations of siSCR PICMs or siSCR/DES PICMs corresponding to 0.009, 0.028, 0.083, 0.25, 0.75, 2.25, 6.25, 12.5, 25, 50, and 100 nM siSCR per well were added. As a positive control, cells were incubated with a medium supplemented with 10% (v/v) DMSO. After 48 h, 37 °C, the medium was replaced against phenol-red free medium (100 µL well^{-1}) plus freshly prepared 20 µL MTT solution (4 mg mL^{-1} in PBS) and incubated for 4 h. At the end of incubation, the medium was carefully discarded and replaced with 150 µL DMSO to solubilize the formed formazan under the exclusion of light for 30 min. Using an Infinite M200Pro spectrofluorometer (TECAN, Männedorf, Switzerland), the optical density (OD) was determined at 570 nm. The OD_{570} of nanoparticle treated cells was normalized with the OD_{570} of cells exposed to equal volumes of PBS alone. Experiments were performed in triplicates.

In Vivo Studies—HCC Model: All animal studies were approved by the local ethics committee on animal care (number G20-1-130, Government of Rhineland Palatinate, Germany). Eight to ten weeks old C57BL/6JRj were purchased from Janvier (Rite du Genest, France) and kept under 12 h light–dark cycles at 25 °C and 40–60% humidity with daily human care. The animals had access to regular chow and water ad libitum. At predetermined time points, mice were sacrificed by cervical dislocation. Dt81Hepa1-6 cells were trypsinated, resuspended in PBS (500 000 cells per 150 µL), and loaded into 21G syringes. Anesthetized (Ketamine/Xylazin after GV solas) mice received right side laparotomy and the spleen was mobilized out of the abdomen for injection. The syringe was inserted into the spleen parenchyma and the cells gently injected. When the spleen regained its red color, the needle was carefully drawn out. The spleen was relocalized into the abdominal cavity and the abdominal cavity was closed with a biodegradable suture and the skin with wound clips. For post-surgical analgesia, the drinking water was supplemented with 1.5 mg mL^{-1} metamizole for 2 days. Following 28 days of tumor growth, mice were sacrificed by cervical dislocation for organ harvest and further analysis.

In Vivo Toxicity: To study the toxicity of the carriers, nanoparticles were loaded with scrambled siRNA (siSCR). Healthy mice were challenged by three consecutive intravenous injections (i.v.) (day 1, 3, and 5) of siSCR PICMs or siSCR/DES PICMs corresponding to escalating doses of siSCR 0.5, 1.0, and 3.0 mg kg^{-1}. As a control, siSCR LNPs were intravenously administrated at a dose of siSCR 1.0 mg kg^{-1}. After 72 h of the last injection mice were anesthetized, blood was sampled by heart puncture and the mice sacrificed by cervical dislocation.

Cytokine levels of interferon (IFN)-α,-β were analyzed by Cytometric Bead Arrays (BD, Heidelberg, Germany) in sera of siSCR(/DES) PICMs or siSCR LNP treated mice as well as healthy untreated mice (as control) according to the manufacturer's protocol. In brief, IFN levels were measured with an Attune NxT flow cytometer (Thermofisher, Waltham, USA) and analyzed using FCAP Array software v.1 (BD, Heidelberg, Germany) according to the manufacturer's instructions. Standard laboratory parameters were analyzed by the central laboratory of the university medical center Mainz, Germany.

In Vivo Imaging: On day 26 post intrasplenic HCC cell (Dt81Hepa1-6) injection, mice received an intravenous injection of Cy5.5-labeled siRNA (siCy5.5) loaded PICMs or siCy5.5/DES PICMs corresponding to a dose of 1.5 mg kg^{-1} siRNA. Control mice received siCy5.5 LNPs or free siCy5.5. At

predetermined time points (0, 1, 3, 6, 24, and 48 h post siCy5.5 (/NP) injection), mice were anesthetized with isoflurane gas and transferred into the imaging chamber of an IVIS (in vivo imaging spectrum) system (Caliper LifeSciences, Hopkinton, USA) for in vivo NIR fluorescence imaging. A picture integration time of 4 s was set for the fluorescence source and filters were adjusted with excitation at 684 nm and emission at 710 nm to visualize the Cy5.5 signal.

Ex Vivo Imaging of Organs: Immediately after the last in vivo NIR-imaging mice were sacrificed by cervical dislocation and lung, heart, liver, spleen, and kidneys retransferred into the imaging chamber of the IVIS Spectrum Imaging system. Image acquisition was performed with the same settings as described above for in vivo imaging. To quantify the fluorescence in individual organs, the extracted organs were carefully circumscribed by regions-of-interest using the IVIS machine software (Caliper LifeSciences, Hopkinton, USA). The fluorescence was quantified as the average of area-normalized radiant efficiency.

Preparation of Liver Single Cell Suspensions: Dissected livers were digested directly after ex vivo imaging according to the manufacturer's protocol (Preparation of single-cell suspensions from mouse liver, Milteny, Bergisch Gladbach, Germany). Briefly, livers were rinsed with Krebs–Ringer–Buffer (KRB, pH7.4) after removal of the gall bladder, digested with 5000 U mL^{-1} of collagenase IV (C5138, Sigma-Aldrich), and 1500 U mL^{-1} DNase I (AppliChem, Darmstadt, Germany) in KRB. The livers were thoroughly minced with a gentle MACS dissociator (Milteny, Bergisch Gladbach, Germany) and incubated for 30 min at 37 °C. Following additional mincing, the cell suspension was filtered over a 100 µM cell strainer to remove debris. The filtrate was centrifuged at 300 g for 10 min at 4 °C to collect both, parenchymal and non-parenchymal cells. The supernatant was discarded and the remaining erythrocytes were lysed with Gey's Buffer (pH7.4) for 1 min at room temperature. Finally, the remaining cells were washed twice with PBS.

In Vivo Biodistribution on Cellular Level in the Liver: Livers, obtained from mice injected with siCy5.5 PICMs or siCy5.5/DES PICMs were processed into single cell suspensions (see above) in order to be stained with fluorochrome-labeled cell-specific antibodies for flow cytometry as described below.

Flow Cytometry: Liver single suspensions (as described above) obtained from biodistribution or therapeutic experiments, were stained with fluorochrome-labeled antibodies according to the manufacturer's protocol. Therefore, the following antibodies were used: leucocytes (CD45-clone 30F11, ThermoFisher Scientific, Waltham, USA), dendritic cells (CD11b-clone M1/70, CD11c (N418, ThermoFisher), macrophages (F4/80-clone BM8, eBiosciences, Darmstadt, Germany), T-cells (CD3- clone 145-2C11, BD, Franklin Lakes, USA), fibroblasts/CAF (α-SMA-clone 1A4, Invitrogen, Carlsbad, USA), HCC-cells (AFP-PE clone 189 502, R&DSystems, Minneapolis, USA) and MFAP-5 (Abcam, Cambridge, UK). To exclude dead cells fixable viability dye (FVD) eFlour 506 (eBioscience, San Diego, USA) was used. Blocking CD16/CD32 (EPR23501-203, Abcam, Cambridge, United Kingdom) prevented unspecific binding. In order to enable intracellular staining, cells were permeabilized using a Foxp3/Transcription factor Staining Buffer Set (eBioscience, San Diego, USA). Following staining according to the manufacturer's protocol, cells were fixed with 4% PFA for 15 min at RT and measured the next day using an Attune NxT Flow Cytometer (ThermoFisher Scientific, Waltham USA). Compensation was performed automatically by Attune NxT Software with OneComp eBeads (eBioscience). 100 000–500 000 cells were measured per sample. Flow cytometry data was analyzed by FlowJo Software v.10.8.1 (BD Biosciences, New Jersey USA).

In Vivo Knockdown of MFAP-5 in HCC Tumor Mice: On day 21 post intrasplenic HCC cell (Dt81Hepa1-6) injections, mice received a total of three consecutive intravenous injections of siMFAP-5 PICMs or siMFAP-5/DES PICMs on day 21, 23, and 25 corresponding to 0.5 and 1.0 mg kg^{-1} siRNA. Mice injected with equal concentrations of complexed siSCR, siMFAP-5 LNPs, or PBS were used as controls. Seventy-two hours after the last injection, mice were sacrificed by cervical dislocation. Lungs, heart, kidneys, livers, and spleens were dissected, and blood collected by heart puncture.

Alpha-Fetoprotein (AFP) Quantification: AFP was quantified in mice sera and cell culture supernatant of Dt81Hepa1-6 and MHSC-SV40 cells, using the Quantikine ELISA-Kit (R&D Systems, Minneapolis, USA) according to the manufacturer's protocol. The provided microplates were precoated with anti-AFP antibodies. Briefly, prediluted sera (1:1000) and standards (each 100 µL $well^{-1}$) added and incubated for 2 h at RT. Following three washing steps (250 µL) with washing buffer, the detection reagent, a peroxidase-conjugated anti-AFP antibody was added (200 µL $well^{-1}$). After ≈20 min, stop solution (2N H_2SO_4) was added (50 µL) and the microplare immediately subjected to the spectrofluorometer. The corresponding photometric analysis was performed with an Infinite M200Pro spectrofluorometer (TECAN, Männedorf, Switzerland).

Hematoxylin and Eosin (H&E) and Sirius Red Staining: Formalin-fixed paraffine-embedded (5 µM; FFPE) specimens of dissected livers were stained with the H&E Staining Kit (Abcam, Cambridge, UK) according to the manufacturer's protocol. Stained sections were mounted with Vitro-Clud (R.Langenbrink, Emmendingen, Germany) and sealed with a coverslip. Microscopy was performed with a Fritz Microscope (PreciPoint, garching b.M., Germany). For morphometric tumor quantification, percentages of the stained area of the whole liver specimen were measured by Image J Software with an adjusted threshold setting. For accurate morphometrical quantification, tissue disruptions and portal areas were excluded. This procedure was repeated twice per sample and resulting numbers were normalized to untreated controls and expressed as normalized means ± SD ($n = 5$ per group, $n = 2$ per sample). A 5 µM representative liver FFPE specimen was stained with Picro-Sirius Red Solution (Abcam, Cambridge, UK) according to the manufacturer's protocol and mounted, sealed, and microphotographed as described above.

Immunohistochemistry: FFPE tissue sections (3 µM) were stained in the Leica BOND Rx autostainer using a rabbit anti-CD34 (Clone: EP373Y) antibody (1:2000, Abcam, ab81289) and CD105 antibody (1:500, Sino Biologicals, 50407-T24). The standard IHC protocol adjusted to 30 min primary antibody incubation with HIER: 20 min ER1 was used. The staining was detected using the BOND Polymer Refined Detection Kit (Leica, DS9800). Images were acquired using Aperio AT2 Slide Scanner (Leica Biosystems) and analyzed with ImageScope software (Version 12.4.3.5008, Leica Bioscience).

Duplex RNA In Situ Hybridization (RNAScope): FFPE tissues were freshly cut into 3 µM-thick sections. RNAscope HD Duplex chromogenic manual assay was performed using mouse *Mfap5* and *Acta2* probes (Advanced Cell Diagnostics, 490 211 and 319 531-C2, respectively), and RNAscope 2.5 HD Duplex Detection kit (Advanced Cell Diagnostics, 322 500) according to the manufacturer-supplied protocol. Counterstaining was performed with hemelaum (acc. to Mayer). Images were acquired using Aperio AT2 Slide Scanner (Leica Biosystems) and analyzed with ImageScope software (Version 12.4.3.5008, Leica Bioscience).

Total RNA Extraction, Library Preparation, and Directional mRNA Sequencing: Total RNA was extracted from fresh frozen specimens of mouse livers using Quiagens RNeasy Mini Kit. Quantity and quality were determined using the Qubit 4 fluorometer with the RNA BR Assay Kit (Invitrogen) and the Agilent Bioanalyzer 2100 system using the RNA Pico Kit. mRNA-focused RNA libraries were prepared using Illumina's TrueSeq stranded mRNA library prep Kit with an input amount of 1 µg total RNA. Poly(A)-positive mRNA transcripts were isolated from total RNA binding to magnetic oligo(d)T beads and subsequently fragmented and reverse transcribed during first and second strand synthesis to yield double-stranded cDNA. The ends of the cDNA molecules were end-repaired and an adenosine overhang was added to all 3′ ends (A-tailing step) to facilitate the ligation of the adapter molecules. These adapters had individual dedicated index sequences and added the Illumina-specific sequences that were needed for amplification, flow cell hybridization, and sequencing. Single index NEXTflex DNA barcodes (8 bp; Perkin Elmer) were used. The final ligation product was amplified via PCR. Intermediate and final library purification steps were done using AMPure XP beads (Beckman Coulter). Final library quantity and quality were done using the Qubit 4 fluorometer with the 1x dsDNA HS AssayKit (Invitrogen) and the Agilent Bioanalyzer 2100 system using the High Sensitivity DNA kit. All mRNA libraries were

sequenced in paired-end mode (2 × 50 nt) on an Illumina NovaSeq instrument resulting in ≈30 × 10^6 distinct sequencing read pairs per library.

Differential Expression Analysis: RNA-seq raw reads were subjected to quality control with FastQC (v0.11.9, www.bioinformatics.braham.ac.uk/projects/fastqc/) and FastQ Screen (v0.15.1)[88] and subsequently processed with kallisto (v0.42.4)[89] and the *Mus musculus* reference GRCm38 (ENSEMBL release 84). Estimated read counts were summarized per gene and used for differential expression analysis with DESeq2 (version 1.34.0).[90] Log2 fold change values after "apeglm" shrinkage were shown.[91] Genes with BH-adjusted *p*-values < 0.05 and |log2 fold change| > 1 were considered as significantly regulated.[92]

Ingenuity Pathway Analysis: The networks analyses were performed with the Ingenuity Pathway Analysis (IPA, Qiagen, Netherlands). For that, differential gene expression data was uploaded and significantly differentially expressed genes with cut-offs of | log2 Fold Change (FC) | >= 1 and false discovery rate (FDR) < 0.05 were selected for analysis.

Statistical Analysis: Data was shown as means ± SD. The comparison was done using a two-way method of ANOVA followed by Bonferroni multiple comparisons tests for multiple comparisons or Kruskal–Wallis H test followed by pairwise Bonferroni-corrected Mann–Whitney U tests for pairwise comparison. For all tests a $\alpha = 0.05$ level was defined as statistically relevant deviations from the respective null hypotheses. Data were analyzed using GraphPad Prism Version 9.5.1 (GraphPad Software, California, US).

Supporting Information

Supporting Information is available from the Wiley Online Library or from the author.

Acknowledgements

P.S., H.Z., and L.S. contributed equally to this work. M.B. and L.K. would like to acknowledge financial support by the German Research Foundation (DFG) within the Collaborative Research Centers SFB1066-3 Project B5, B8, B12, and B17. The authors would like to thank M. Bilodeau and Dominik Siegl for providing the Dt81Hepa1-6 cell line (HCC cells).

Conflict of Interest

M.B. is a scientific advisory board member of Curapath (Valencia, Spain). L.K. declares receiving travel expenses and speaker honoraria from Gilead science (Foster city, USA) and Takeda (Doshomachi, Japan).

Data Availability Statement

The data that support the findings of this study are available from the corresponding author upon reasonable request.

Keywords

desloratadine, endosomal escape, hepatocellular carcinoma, polyion complex micelles, polypept(o)ides, siRNA co-delivery

Received: April 2, 2024
Revised: May 27, 2024
Published online: July 3, 2024

[1] Y. Miao, Y. Chen, D. Mi, *Heliyon* **2022**, *8*, e11035.
[2] A. Ascione, L. Fontanella, M. Imparato, L. Rinaldi, M. De Luca, *Liver Int.* **2017**, *37*, 1193.
[3] J. M. Llovet, R. K. Kelley, A. Villanueva, A. G. Singal, E. Pikarsky, S. Roayaie, R. Lencioni, K. Koike, J. Zucman-Rossi, R. S. Finn, *Nat. Rev. Dis. Primers* **2021**, *7*, 6.
[4] J. K. H. Liu, A. F. Irvine, R. L. Jones, A. Samson, *Cancer Med.* **2022**, *11*, 571.
[5] R. S. Finn, S. Qin, M. Ikeda, P. R. Galle, M. Ducreux, T.-Y. Kim, M. Kudo, V. Breder, P. Merle, A. O. Kaseb, D. Li, W. Verret, D.-Z. Xu, S. Hernandez, J. Liu, C. Huang, S. Mulla, Y. Wang, H. Y. Lim, A. X. Zhu, A.-L. Cheng, *N. Engl. J. Med.* **2020**, *382*, 1894.
[6] Z. Guizhen, J. Guanchang, L. Liwen, W. Huifen, R. Zhigang, S. Ranran, Y. Zujiang, *Front. Endocrinol.* **2022**, *13*, 918869.
[7] J. D. Yang, I. Nakamura, L. R. Roberts, *Semin. Cancer Biol.* **2011**, *21*, 35.
[8] S. Santagata, G. Rea, D. Castaldo, M. Napolitano, A. Capiluongo, C. D'Alterio, A. M. Trotta, C. Ieranò, L. Portella, S. Di Maro, F. Tatangelo, V. Albino, R. Guarino, C. Cutolo, F. Izzo, S. Scala, *Hepatol. Int.* **2023**, *18*, 568.
[9] J. Zhang, C. Gu, Q. Song, M. Zhu, Y. Xu, M. Xiao, W. Zheng, *Cell Biosci.* **2020**, *10*, 127.
[10] B. Feng, J. Wu, B. Shen, F. Jiang, J. Feng, *Cancer Cell Int.* **2022**, *22*, 166.
[11] R. Mhaidly, F. Mechta-Grigoriou, *Immunol. Rev.* **2021**, *302*, 259.
[12] X. Han, Y. Xu, M. Geranpayehvaghei, G. J. Anderson, Y. Li, G. Nie, *Biomaterials* **2020**, *232*, 119745.
[13] Y. Wu, P. Wu, Q. Zhang, W. Chen, X. Liu, W. Zheng, *Cell Biosci.* **2019**, *9*, 24.
[14] Z. Chen, X. Yan, K. Li, Y. Ling, H. Kang, *Clin. Transl. Oncol.* **2020**, *22*, 522.
[15] C. S. Craft, T. J. Broekelmann, R. P. Mecham, *Matrix Biol.* **2018**, *71*, 100.
[16] J. Jászai, M. H. H. Schmidt, *Cells* **2019**, *8*, 1102.
[17] C. S. Leung, T. L. Yeung, K. P. Yip, S. Pradeep, L. Balasubramanian, J. Liu, K. K. Wong, L. S. Mangala, G. N. Armaiz-Pena, G. Lopez-Berestein, A. K. Sood, M. J. Birrer, S. C. Mok, *Nat. Commun.* **2014**, *5*, 5092.
[18] Q. Zhang, J. Wu, X. Bai, T. Liang, *Front Med (Lausanne)* **2020**, *7*, 584250.
[19] D. Adams, A. Gonzalez-Duarte, W. D. O'Riordan, C.-C. Yang, M. Ueda, A. V. Kristen, I. Tournev, H. H. Schmidt, T. Coelho, J. L. Berk, K.-P. Lin, G. Vita, S. Attarian, V. Planté-Bordeneuve, M. M. Mezei, J. M. Campistol, J. Buades, T. H. Brannagan, B. J. Kim, J. Oh, Y. Parman, Y. Sekijima, P. N. Hawkins, S. D. Solomon, M. Polydefkis, P. J. Dyck, P. J. Gandhi, S. Goyal, J. Chen, A. L. Strahs, et al., *N. Engl. J. Med.* **2018**, *379*, 11.
[20] W. Alshaer, H. Zureigat, A. Al Karaki, A. Al-Kadash, L. Gharaibeh, M. M. Hatmal, A. A. A. Aljabali, A. Awidi, *Eur. J. Pharmacol.* **2021**, *905*, 174178.
[21] R. Kanasty, J. R. Dorkin, A. Vegas, D. Anderson, *Nat. Mater.* **2013**, *12*, 967.
[22] Y. Dong, D. J. Siegwart, D. G. Anderson, *Adv. Drug Delivery Rev.* **2019**, *144*, 133.
[23] H. J. Kim, A. Kim, K. Miyata, K. Kataoka, *Adv. Drug Delivery Rev.* **2016**, *104*, 61.
[24] T. F. Martens, K. Remaut, J. Demeester, S. C. De Smedt, K. Braeckmans, *Nano Today* **2014**, *9*, 344.
[25] D. Ma, *Nanoscale* **2014**, *6*, 6415.
[26] T. Van de Vyver, B. Bogaert, L. De Backer, F. Joris, R. Guagliardo, J. Van Hoeck, P. Merckx, S. Van Calenbergh, S. Ramishetti, D. Peer, K. Remaut, S. C. De Smedt, K. Raemdonck, *ACS Nano* **2020**, *14*, 4774.
[27] C. Muntean, E. Blondeel, L. Harinck, K. Pednekar, J. Prakash, O. De Wever, J. L. Chain, S. C. De Smedt, K. Remaut, K. Raemdonck, *Int. J. Pharm.* **2023**, *644*, 123348.
[28] B. Bogaert, A. Debisschop, T. Ehouarne, H. P. Van Eeckhoutte, J. De Volder, A. Jacobs, E. Pottie, R. De Rycke, A. Crabbé, P. Mestdagh, I. Lentacker, G. G. Brusselle, C. Stove, S. Verstraelen, T. Maes, K. R. Bracke, S. C. De Smedt, K. Raemdonck, *Nano Lett.* **2023**, *24*, 2961.

[29] L. Capelôa, M. Yazdi, H. Zhang, X. Chen, Y. Nie, E. Wagner, U. Lächelt, M. Barz, *Macromol. Rapid Commun.* **2022**, *43*, 2100698.
[30] A. Birke, D. Huesmann, A. Kelsch, M. Weilbächer, J. Xie, M. Bros, T. Bopp, C. Becker, K. Landfester, M. Barz, *Biomacromolecules* **2014**, *15*, 548.
[31] K. Klinker, M. Barz, *Macromol. Rapid Commun.* **2015**, *36*, 1943.
[32] H. R. Kricheldorf, *Angew. Chem., Int. Ed.* **2006**, *45*, 5752.
[33] A. Birke, J. Ling, M. Barz, *Prog. Polym. Sci.* **2018**, *81*, 163.
[34] T. J. Deming, *Nature* **1997**, *390*, 386.
[35] T. J. Deming, in *Peptide Hybrid Polymers*, Springer-Verlag, Berlin/Heidelberg **2006**, pp. 1–18.
[36] K. Shiraishi, M. Yokoyama, *Sci. Technol. Adv. Mater.* **2019**, *20*, 324.
[37] W. Najahi-Missaoui, R. D. Arnold, B. S. Cummings, *Int. J. Mol. Sci.* **2021**, *22*, 385.
[38] T. Thanh, H. Thi, E. H. Pilkington, D. H. Nguyen, J. S. Lee, *Polymers* **2020**, *12*, 298.
[39] S. S. Nogueira, A. Schlegel, K. Maxeiner, B. Weber, M. Barz, M. A. Schroer, C. E. Blanchet, D. I. Svergun, S. Ramishetti, D. Peer, P. Langguth, U. Sahin, H. Haas, *ACS Appl. Nano Mater.* **2020**, *3*, 10634.
[40] I. Alberg, S. Kramer, M. Schinnerer, Q. Hu, C. Seidl, C. Leps, N. Drude, D. Möckel, C. Rijcken, T. Lammers, M. Diken, M. Maskos, S. Morsbach, K. Landfester, S. Tenzer, M. Barz, R. Zentel, *Small* **2020**, *16*, 1907574.
[41] E. Hara, M. Ueda, C. J. Kim, A. Makino, I. Hara, E. Ozeki, S. Kimura, *J. Pept. Sci.* **2014**, *20*, 570.
[42] K. Johann, T. Bohn, F. Shahneh, N. Luther, A. Birke, H. Jaurich, M. Helm, M. Klein, V. K. Raker, T. Bopp, M. Barz, C. Becker, *Nat. Commun.* **2021**, *12*, 5981.
[43] T. A. Bauer, N. K. Horvat, O. Marques, S. Chocarro, C. Mertens, S. Colucci, S. Schmitt, L. M. Carrella, S. Morsbach, K. Koynov, F. Fenaroli, P. Blümler, M. Jung, R. Sotillo, M. W. Hentze, M. U. Muckenthaler, M. Barz, *Adv. Healthcare Mater.* **2021**, *10*, 2100385.
[44] I. Negwer, A. Best, M. Schinnerer, O. Schäfer, L. Capeloa, M. Wagner, M. Schmidt, V. Mailänder, M. Helm, M. Barz, H. J. Butt, K. Koynov, *Nat. Commun.* **2018**, *9*, >5306.
[45] P. M. Klein, K. Klinker, W. Zhang, S. Kern, E. Kessel, E. Wagner, M. Barz, *Polymers* **2018**, *10*, 10.
[46] T. A. Bauer, J. Imschweiler, C. Muhl, B. Weber, M. Barz, *Biomacromolecules* **2021**, *22*, 2171.
[47] B. Lacoste, V. A. Raymond, S. Cassim, P. Lapierre, M. Bilodeau, *PLoS One* **2017**, *12*, 0171215.
[48] A. Birke, J. Ling, M. Barz, *Prog. Polym. Sci.* **2018**, *81*, 163.
[49] D. Huesmann, A. Birke, K. Klinker, S. Türk, H. J. Räder, M. Barz, *Macromolecules* **2014**, *47*, 928.
[50] B. Weber, A. Birke, K. Fischer, M. Schmidt, M. Barz, *Macromolecules* **2018**, *51*, 2653.
[51] P. Heller, B. Weber, A. Birke, M. Barz, *Macromol. Rapid Commun.* **2015**, *36*, 38.
[52] P. Heller, N. Mohr, A. Birke, B. Weber, A. Reske-Kunz, M. Bros, M. Barz, *Macromol. Biosci.* **2015**, *15*, 63.
[53] C. Kappel, C. Seidl, C. Medina-Montano, M. Schinnerer, I. Alberg, C. Leps, J. Sohl, A. K. Hartmann, M. Fichter, M. Kuske, J. Schunke, G. Kuhn, I. Tubbe, D. Paßlick, D. Hobernik, R. Bent, K. Haas, E. Montermann, K. Walzer, M. Diken, M. Schmidt, R. Zentel, L. Nuhn, H. Schild, S. Tenzer, V. Mailänder, M. Barz, M. Bros, S. Grabbe, *ACS Nano* **2021**, *15*, 15191.
[54] O. Schäfer, K. Klinker, L. Braun, D. Huesmann, J. Schultze, K. Koynov, M. Barz, *ACS Macro Lett.* **2017**, *6*, 1140.
[55] S. Beck, J. Schultze, H.-J. Räder, R. Holm, M. Schinnerer, M. Barz, K. Koynov, R. Zentel, *Polymers* **2018**, *10*, 141.
[56] E. J. L. Stéen, J. T. Jørgensen, K. Johann, K. Nørregaard, B. Sohr, D. Svatunek, A. Birke, V. Shalgunov, P. E. Edem, R. Rossin, C. Seidl, F. Schmid, M. S. Robillard, J. L. Kristensen, H. Mikula, M. Barz, A. Kjær, M. M. Herth, *ACS Nano* **2020**, *14*, 568.
[57] P. Heller, D. Hobernik, U. Lächelt, M. Schinnerer, B. Weber, M. Schmidt, E. Wagner, M. Bros, M. Barz, *J. Controlled Release* **2017**, *258*, 146.
[58] J. Kornhuber, M. Muehlbacher, S. Trapp, S. Pechmann, A. Friedl, M. Reichel, C. Mühle, L. Terfloth, T. W. Groemer, G. M. Spitzer, K. R. Liedl, E. Gulbins, P. Tripal, *PLoS One* **2011**, *6*, e23852.
[59] A. M. Villamil Giraldo, H. Appelqvist, T. Ederth, K. Öllinger, *Biochem. Soc. Trans.* **2014**, *42*, 1460.
[60] F. Joris, L. De Backer, T. Van de Vyver, C. Bastiancich, S. C. De Smedt, K. Raemdonck, *J. Controlled Release* **2018**, *269*, 266.
[61] T. Van de Vyver, S. C. De Smedt, K. Raemdonck, *Adv. Drug Delivery Rev.* **2022**, *181*, 114041.
[62] T. Van de Vyver, B. Bogaert, L. De Backer, F. Joris, R. Guagliardo, J. Van Hoeck, P. Merckx, S. Van Calenbergh, S. Ramishetti, D. Peer, K. Remaut, S. C. De Smedt, K. Raemdonck, *ACS Nano* **2020**, *14*, 4774.
[63] Z. U. Rehman, D. Hoekstra, I. S. Zuhorn, *ACS Nano* **2013**, *7*, 3767.
[64] L. M. P. Vermeulen, T. Brans, S. K. Samal, P. Dubruel, J. Demeester, S. C. De Smedt, K. Remaut, K. Braeckmans, *ACS Nano* **2018**, *12*, 2332.
[65] S. Principe, S. Mejia-Guerrero, V. Ignatchenko, A. Sinha, A. Ignatchenko, W. Shi, K. Pereira, S. Su, S. H. Huang, B. O'Sullivan, W. Xu, D. P. Goldstein, I. Weinreb, L. Ailles, F. F. Liu, T. Kislinger, *J. Proteome Res.* **2018**, *17*, 2045.
[66] S. Principe, S. Mejia-Guerrero, V. Ignatchenko, A. Sinha, A. Ignatchenko, W. Shi, K. Pereira, S. Su, S. H. Huang, B. O'Sullivan, W. Xu, D. P. Goldstein, I. Weinreb, L. Ailles, F.-F. Liu, T. Kislinger, *J. Proteome Res.* **2018**, *17*, 2045.
[67] D. Öhlund, E. Elyada, D. Tuveson, *J. Exp. Med.* **2014**, *211*, 1503.
[68] F. Wu, J. Yang, J. Liu, Y. Wang, J. Mu, Q. Zeng, S. Deng, H. Zhou, *Signal Transduction Targeted Ther.* **2021**, *6*, 218.
[69] L. Kaps, D. Schuppan, *Cells* **2020**, *9*, 2027.
[70] T. L. Yeung, C. S. Leung, K. P. Yip, J. Sheng, L. Vien, L. C. Bover, M. J. Birrer, S. T. C. Wong, S. C. Mok, *Clin. Cancer Res.* **2019**, *25*, 6417.
[71] Z. Jia, Y. Wang, A. Sawyers, H. Yao, F. Rahmatpanah, O. Q. Xia, Q. Xu, R. Pio, T. Turan, J. A. Koziol, S. Goodison, P. Carpenter, J. Wang-Rodriguez, A. Simoneau, F. Meyskens, M. Sutton, W. Lernhardt, T. Beach, J. Monforte, M. McClelland, D. Mercola, *Cancer Res.* **2011**, *71*, 2476.
[72] B. Li, E. Severson, J. C. Pignon, H. Zhao, T. Li, J. Novak, P. Jiang, H. Shen, J. C. Aster, S. Rodig, S. Signoretti, J. S. Liu, X. S. Liu, *Genome Biol.* **2016**, *17*, 174.
[73] T. Li, J. Fan, B. Wang, N. Traugh, Q. Chen, J. S. Liu, B. Li, X. S. Liu, *Cancer Res.* **2017**, *77*, e108.
[74] F. Wu, J. Yang, J. Liu, Y. Wang, J. Mu, Q. Zeng, S. Deng, H. Zhou, *Signal Transduction Targeted Ther.* **2021**, *6*, 218.
[75] N. Leber, L. Kaps, M. Aslam, J. Schupp, A. Brose, D. Schäffel, K. Fischer, M. Diken, D. Strand, K. Koynov, A. Tuettenberg, L. Nuhn, R. Zentel, D. Schuppan, *J. Controlled Release* **2017**, *248*, 10.
[76] L. Kaps, L. Nuhn, M. Aslam, A. Brose, F. Foerster, S. Rosigkeit, P. Renz, R. Heck, Y. O. Kim, I. Lieberwirth, D. Schuppan, R. Zentel, *Adv. Healthcare Mater.* **2015**, *4*, 2809.
[77] S. M. Moghimi, R. McCullough, D. Simberg, *Mol. Ther.* **2023**, *31*, 605.
[78] D. Witzigmann, J. A. Kulkarni, J. Leung, S. Chen, P. R. Cullis, R. van der Meel, *Adv. Drug Delivery Rev.* **2020**, *159*, 344.
[79] T. Liu, C. Han, S. Wang, P. Fang, Z. Ma, L. Xu, R. Yin, *J. Hematol. Oncol.* **2019**, *12*, 86.
[80] L. D. Ferrell, S. Kakar, L. M. Terracciano, A. Wee, in *MacSween's Pathology of the Liver*, Elsevier Inc., Philadelphia **2018**, pp. 780–879.
[81] A. Nogués, E. Gallardo-Vara, M. P. Zafra, P. Mate, J. L. Marijuan, A. Alonso, L. M. Botella, M. I. Prieto, *World J. Surg. Oncol.* **2020**, *18*, 99.
[82] F. Foerster, S. Boegel, R. Heck, G. Pickert, N. Rüssel, S. Rosigkeit, M. Bros, S. Strobl, L. Kaps, M. Aslam, M. Diken, J. Castle, U. Sahin, A. Tuettenberg, E. Bockamp, D. Schuppan, *Oncoimmunology* **2018**, *7*, 1409929.

[83] L. Kaps, A. Huppertsberg, N. Choteschovsky, A. Klefenz, F. Durak, B. Schr€, M. Diken, E. Eichler, S. Rosigkeit, S. Schmitt, C. Leps, A. Schulze, F. Foerster, E. Bockamp, B. G. De Geest, K. Koynov, H.-J. R€, S. Tenzer, F. Marini, D. Schuppan, L. Nuhn, K. Wooley, **2022**, *119*, 2122310119.
[84] H. E. Gottlieb, V. Kotlyar, A. Nudelman, *J. Org. Chem.* **1997**, *62*, 7512.
[85] P. Heller, D. Hobernik, U. Lächelt, M. Schinnerer, B. Weber, M. Schmidt, E. Wagner, M. Bros, M. Barz, *J. Controlled Release* **2017**, *258*, 146.
[86] O. Schäfer, D. Huesmann, C. Muhl, M. Barz, *Chemistry* **2016**, *22*, 18085.
[87] A. Werner, M. Koschke, N. Leuchtner, C. Luckner-Minden, A. Habermeier, J. Rupp, C. Heinrich, R. Conradi, E. I. Closs, M. Munder, *Front. Immunol.* **2017**, *8*, 864.
[88] S. W. Wingett, S. Andrews, *F1000Res* **2018**, *7*, 1338.
[89] N. L. Bray, H. Pimentel, P. Melsted, L. Pachter, *Nat. Biotechnol.* **2016**, *34*, 525.
[90] M. I. Love, W. Huber, S. Anders, *Genome Biol.* **2014**, *15*, 550.
[91] A. Zhu, J. G. Ibrahim, M. I. Love, *Bioinformatics* **2019**, *35*, 2084.
[92] Y. Benjamini, Y. Hochberg, *Controlling the False Discovery Rate: A Practical and Powerful Approach to Multiple Testing*, **1995**.